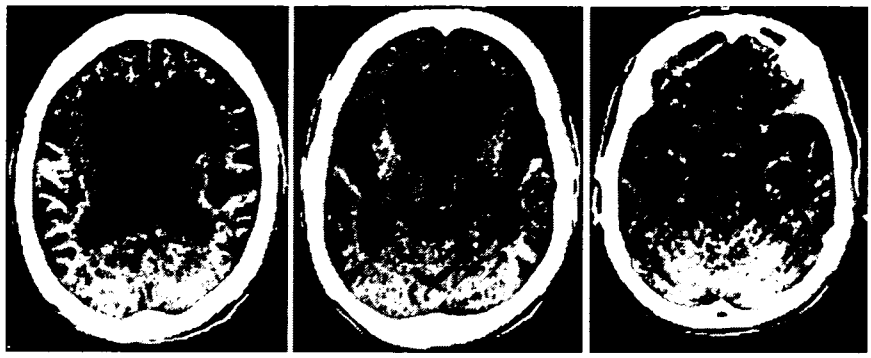

Fig. 1 CT scan at the age of 48 years, showing severe cerebral atrophy with fronto-temporal predominance.

were cut on a freezing microtome at 30 μm and treated as a free-floating sections. The primary antibodies employed in this study were mouse monoclonal anti-3R-tau, anti-4R-tau antibodies (RD3 and RD4, respectively)[12,13], anti-human-tau or AT-8. For immunostaining of formalin-fixed paraffin-embedded blocks with RD3 (1:100) or RD4 (1:100), the sections were pretreated in 70% formic acid for 10 min, and autoclaved in 0.01 mol/L citrate buffer (pH 6.0) at 120°C for 10 min. The floating sections fixed with 4% PFA were pretreated in 99% formic acid for 30 min for staining with RD3 (1:200), and autoclaved for 10 min for staining with RD4 (1:200). Primary antibody labeling was detected using the ABC system (Vector Laboratory, Burlingame, CA, USA) coupled with a diaminobenzidine (DAB) reaction intensified with nickel ammonium sulfate to yield a dark-purple precipitate. After immunostaining, sections were briefly counter-stained with nuclear fast red.

RESULTS

General autopsy findings

A large multilobular cyst was noticed in the right ovary. Most of its contents were bloody serum (300 mL), and abscess formation was noted in part of the cyst.

Neuropathological findings

Gross findings

After fixation, the brain weighed 530 g. No marked changes were observed in the pia mater of the brain, and no atheromatous degeneration was noted in the vertebral or basilar artery. The cerebrum was markedly atrophied, especially in the frontal and temporal lobes, and the atrophy had spread to the parietal and occipital lobes. In the frontal lobe, atrophy was marked in the superior, middle and inferior frontal gyri, cingulate and rectal gyri. However, the orbital gyrus, the precentral gyrus and the latter half of the inferior frontal gyrus were relatively preserved.

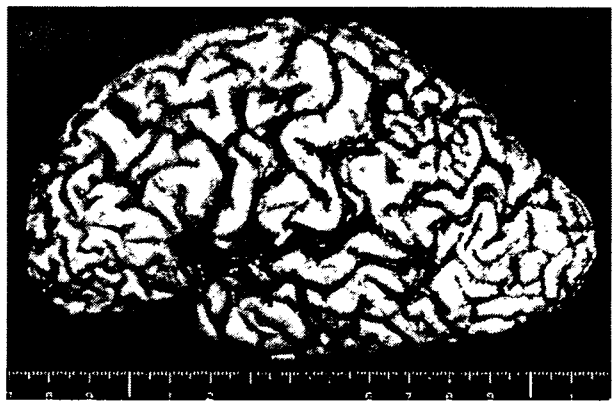

Fig. 2 Lateral view of the right cerebrum, showing marked atrophy of the fronto-temporal lobes. The parietal and occipital lobes are also atrophied.

In the temporal lobe, atrophy was predominant in the anterior region; intense atrophy was noted in the superior, middle and inferior temporal gyri, the fusiform, parahippocampal and hippocampal gyri. The latter half of the superior temporal gyrus was relatively preserved. In the parietal lobe, atrophy affected the angular and supramarginal gyri, but the postcentral gyrus was relatively preserved. In the occipital lobe, atrophy had spread to the medial occipitotemporal gyrus, but the calcarine cortex was spared. The brainstem was also atrophic. The cerebellum was slightly reduced in size. On coronal-section, the lateral ventricles were markedly enlarged, and the cerebral cortex and white matter were remarkably thinned. Degeneration in the superior temporal gyrus, transverse gyrus, and striate area, including the white matter, were relatively mild. In the white matter, diffuse gelatinous degeneration was noted, except for a portion of the occipital lobe, which was not hardened, even after formalin fixation, and was pale brown and translucent. The hippocampus, amygdala, basal ganglia and thalamus were severely atrophied. In cross-section, the mesencephalon and each part of the brainstem were atrophied, and the substantia nigra and locus ceruleus were depigmented (Figs 2–4).

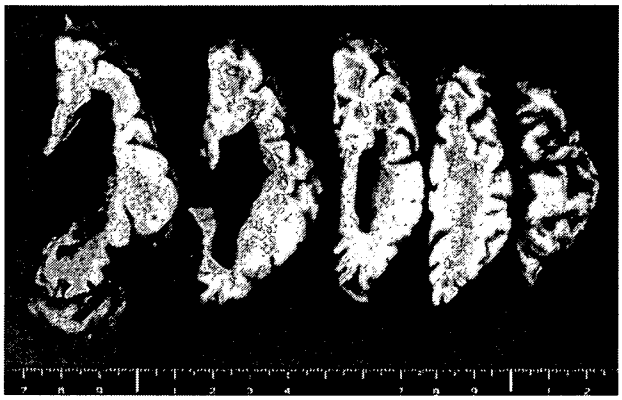

Fig. 3 Coronal-section of the frontal lobe, showing severe cortical atrophy and diffuse gelatinous degeneration of the white matter.

Microscopic findings

In the cerebral cortex, marked neuronal loss was noted, and destruction of the cell structure was remarkable. Even in the superior temporal gyrus, transverse gyrus, and striate area, which grossly appeared relatively intact, the thickness of the cortex was reduced, and small neurons were mostly atrophic, although a relatively small percentage of them were lost. A spongy state was observed primarily in the two superficial layers. A large number of intracytoplasmic inclusions (Pick bodies) were identified by Bodian staining, and were most numerous in the third layer, followed by the fifth layer, including area 17. There were a few ballooned neurons. No senile plaques were noted, and gliosis was diffusely observed in the cortex, but was more notable near the surface. In the hippocampus, NFT were detected in the pyramidal cell layer by Gallyas staining, and there were also many Pick bodies. In the granular cell layer of the dentate gyrus, numerous Pick bodies were observed. In the white matter, the destruction of the myelin sheaths and axons was notable. In Holzer staining, fibrillary gliosis was not noticed in the softened gelatinous white matter, but marked gliosis was observed as a thin band in the subcortical white matter. Oligodendroglial inclusions (coiled bodies) were also encountered, and were more numerous in areas where gelatinous degeneration was milder. The internal and external capsules were markedly reduced in thickness, and severe gliosis was detected along the fibers. In the thalamus, the loss of neurons, Pick bodies and severe gliosis were noted in the medial nucleus, ventral lateral nucleus, and dorsal lateral nucleus.

In the basal ganglia, the large and small cells of the caudate nucleus were moderately reduced in number, and many of them contained Pick bodies. In the putamen, there was a moderate loss of neurons, mild gliosis and Pick bodies. A mild loss of neurons, moderate gliosis, and Pick bodies were noted in the pallidum, and a large number of pigmented granules were observed in the matrix. Neuronal loss and Pick bodies were observed in the amygdala, and marked gliosis was demonstrated by the Holzer stain prominently in the basolateral group. In the subthalamic nucleus and Meynert's nucleus, Pick bodies were noted, but the number of neurons remained nearly intact.

In the mesencephalon, there were many Pick bodies in the red nuclei, substantia nigra and periaqueductal gray matter. In the pons, a large number of Pick bodies and marked gliosis were present in the pontine nuclei. In the cerebellum, the Purkinje cell layer, molecular layer, granular layer and white matter were mostly intact. In the dentate nucleus, a mild loss of neurons, grumose degeneration and many Pick bodies were observed. In the medulla oblongata, many Pick bodies were noted in the reticular nuclei. A large number of Pick bodies were present in the dorsal nucleus of the vagus and hypoglossal nucleus, but the number of neurons was relatively preserved. In the thoracic spinal cord and lumbar spinal cord, the loss of neurons was slight, but gliosis was present, and numerous Pick bodies were observed. The Clarke's column showed the loss of neurons, gliosis and numerous Pick bodies. There was also degeneration of the pyramidal tract; the degeneration was more marked in the spinal cord than in the medulla oblongata and posterior fasciculus.

By immunohistochemistry, Pick bodies, NFT, and oligodendroglial coiled bodies were stained with antihuman tau, AT8 and RD3. RD4 did not stain most of these structures except for a few NFT in the CA1 of the hippocampus. Similar findings were obtained by immunostaining of formalin-fixed paraffin-embedded specimens (Figs 5,6).

DISCUSSION

In the autopsied brain of this case, severe atrophy, involving all cerebral lobes, with fronto-temporal predominance was macroscopically observed. Histological examination showed the loss of neurons in all layers in an extensive area of the cerebral cortex, but relatively well-preserved neurons in the inferior frontal gyrus and superior temporal gyrus, and calcarine cortex, consistent with the degeneration pattern in Pick's disease. There were no senile plaques, and NFT were localized in the hippocampal region, which excluded Alzheimer's disease. The white matter showed extensive gelatin-like degeneration, positively indicating an anoxic change that took place during the clinical course of this case. The time that it developed was unknown. In neurons, Pick bodies were observed in extensive areas from the cerebral cortex to the spinal cord. In the cerebral cortex, ballooned neurons were also present.

Pick bodies were identified by Bodian staining and were stainable with the anti-3R-tau antibody, but not with

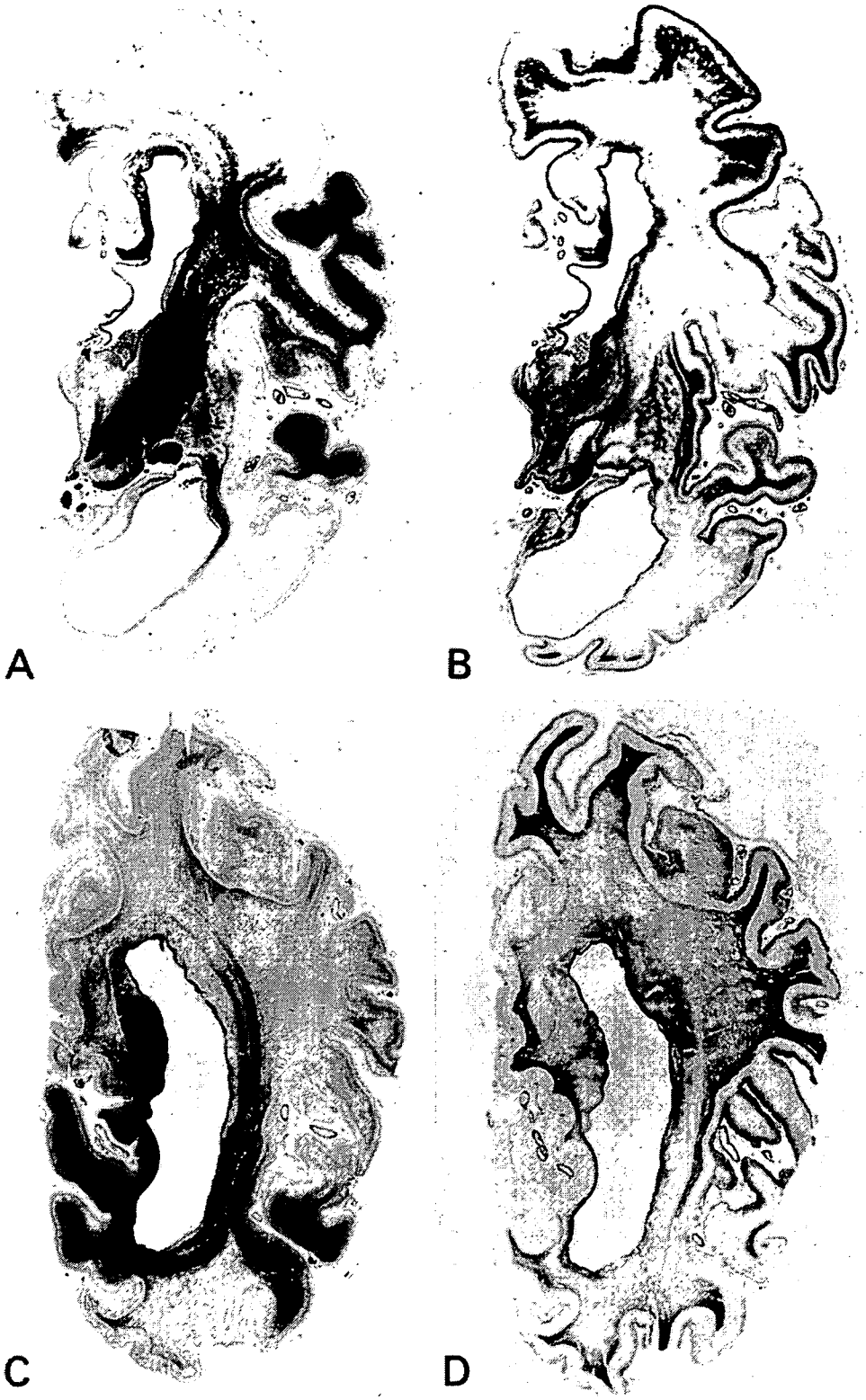

Fig. 4 Severe involvement of the fronto-temporal lobes (A, B) and parieto-occipital lobes (C, D), except for the superior temporal gyrus and the area 17. (A, C: Klüver-Barrera; B, D: Holzer).

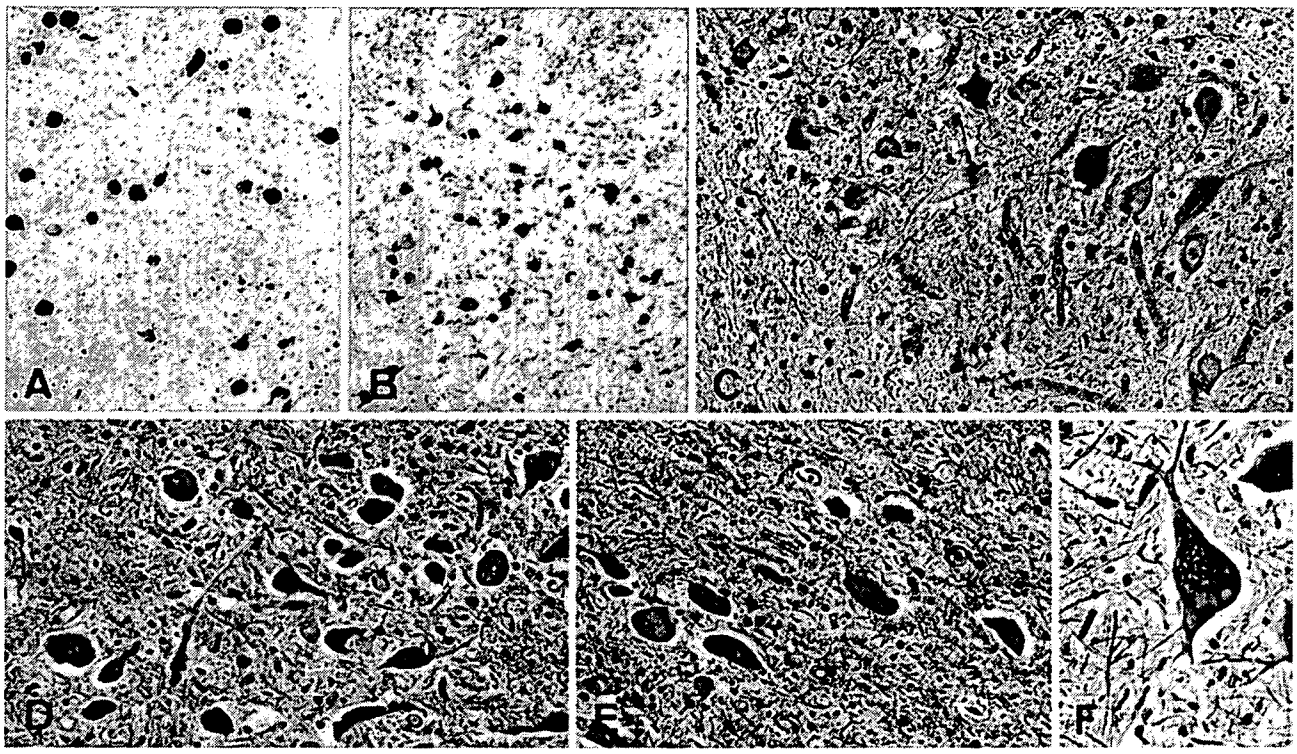

Fig. 5 Pick bodies in the Meynert's nucleus (A, AT-8 immunochemistry ×100), and pontine nuclei (B, antihuman-tau immunochemistry ×100). Dentate nucleus, showing grumose degeneration in the presence of Pick bodies (C, Bodian ×200). Pick bodies in the dorsal nucleus of the vagus (D, Bodian ×200), hypoglossal nucleus (E, Bodian ×200) and anterior horn of the thoracic medulla (F, Bodian ×250).

the anti-4R-tau antibody in immunostaining. Based on these findings, the argyrophilic intraneuronal inclusions observed in this case are typical Pick bodies.[10] Moreover, similar tau staining pattern of oligodendroglial coiled bodies to that of Pick bodies suggests that they also consist exclusively of 3R-tau. These results are consistent with previous reports that argued tau isoform specific pathology takes place in both neurons and oligodendrocytes in Pick's disease.[14]

In this case, the brain weighed 530 g. To our knowledge, this is the lowest weight in cases of not only Pick's disease, but also fronto-temporal lobar degeneration as a comprehensive disease concept or Pick complex, including associated diseases. Kosaka *et al.* evaluated 60 autopsy cases of Pick's disease (including Pick's disease without Pick bodies) and observed only two cases with brainweights less than 800 g, and their review of other cases showed that a brainweight of less than 800 g is rare.[15] The brainweight tended to decrease with the duration of the disease. Although the duration of the disease was also long (10 years and 8 months) in this case, the low brainweight was remarkable.

The important finding in this case was the distribution of Pick bodies. Numerous Pick bodies were observed not only in all the cerebral cortices, but also various subcortical nuclei, including the dentate nucleus, dorsal nucleus of the vagus, hypoglossal nucleus, anterior horn cells, and Clarke's column in the spinal cord, in addition to the usual distribution areas. Arima evaluated the distribution of Pick bodies in seven cases of PDPB and observed rare Pick bodies in the dentate nucleus and dorsal nucleus of the vagus in only one case, and no Pick bodies in the spinal cord.[16]

On clinical symptoms, the medical records for this patient taken at Hospital A show that this case was initially manifested by headaches and memory disturbance. These were followed by personality and emotional disorders, and symptoms characteristic of Pick's disease, such as "Stehende Redensarten" and Klüver–Bucy syndrome, which developed during the subsequent course. She had lost almost all language ability 3 years after disease onset and showed an apallic state 6 years after disease onset. The progression of the clinical condition until then was rather rapid for Pick's disease, but the course until this period was considered to be typical.[17] However, this patient showed bulging eyes in her clinical course, and developed myoclonus of the trunk 7 years after onset, which persisted for more than 3 years until her death. The myoclonus seen in this patient can be considered to be reflex myoclonus since

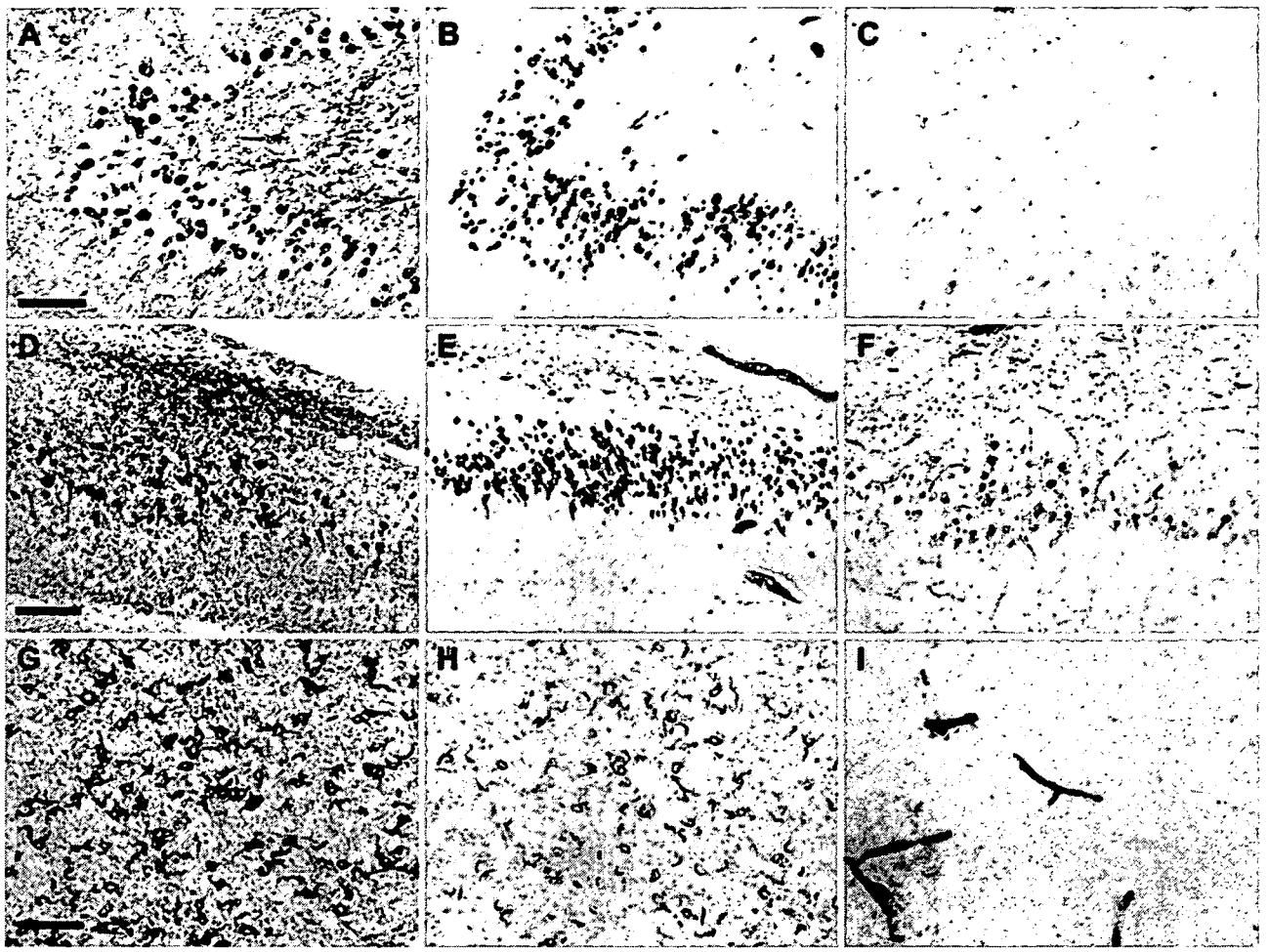

Fig. 6 Immunostaining of the granular cell layer of the dentate gyrus (A–C), the pyramidal cell layer of the CA1 (D–F), and the white matter of the temporal lobe (G–I), using AT8 (A, D, and G), RD3 (B, E, and H), and RD4 (C, F, and I). Numerous Pick bodies in the granular cells of the dentate gyrus are positive for AT8 (A) and RD3 (B), but are negative for RD4 (C). In the CA1 of the hippocampus, a lot of Pick bodies and NFT are stained with AT8 (D) and RD3. With RD4, only a few NFT are stained (F). In the white matter of the temporal lobe, massive oligodendroglial coiled bodies are positive for AT8 (G) and RD3 (H), but are negative for RD4 (I). Positive staining of the capillaries for RD4 (I) may represent its cross-reactivity to some blood components. Bars A (also for B and C) 100 μm; D (also for E and F) 200 μm; G (also for H and I) 50 μm.

it developed in response to stimulation. Furthermore, since it was accompanied by an evident emotional response, the myoclonus in this case seemed to be associated with the startle response.[18] EEG did not reveal known myoclonus-associated signs, for example, periodic synchronous discharge, or polyspike and wave complexes specific to myoclonic seizure.

Bulging eyes are known to be a characteristic feature of Machado-Joseph disease. Iwabuchi *et al.* speculated that bulging eyes are attributed to eyelid dystonia.[19] This view is based on the finding that bulging eyes are also seen in patients with blepharoptosis. According to this view, in the present case, the degeneration of the extrapyramidal system was more marked as compared to typical cases of PDPB, and it seems possible that this degeneration induced bulging eyes.

Myoclonus is generally absent in Pick's disease and was reported by Neary *et al.* as exclusion criteria for the diagnosis of fronto-temporal lobar degeneration.[20] In Alzheimer's disease, the incidence of myoclonus is considerably high. The incidence has been frequently reported to be approximately 10% or more. Hauser *et al.* observed myoclonus in eight of 81 autopsy cases of dementia of Alzheimer's type.[21] Risse *et al.* performed a follow-up survey of cases of clinically probable Alzheimer's disease until autopsy and observed myoclonus in 55% of cases in which a definite pathological diagnosis was made.[22] The pathological basis of myoclonus in Alzheimer's disease has not yet

been established. Some studies have suggested the dentate nuclei to be the responsible lesion. The pathological basis of myoclonus has been suggested to be a grumose degeneration of the dentate nuclei or the ratio of small/large neurons in the damaged dentate nuclei.[23,24] In this patient, grumose degeneration of the dentate nucleus, which is not generally observed in Pick's disease, was also observed.

Among the cerebral cortical lesions associated with Pick's disease, atrophy confined to the frontal and temporal lobes has been emphasized. However, approximately half a century ago, Lüers and Spatz already noted that involvement of the parietal lobe is not rare in Pick's disease.[25] Recently, Tsuchiya *et al.* reported that the cerebral cortical lesions associated with PDPB show diverse distribution, and that the cerebral cortical lesions in PDPB are more widespread than previously assumed.[26] Therefore, atypical cases of PDPB, expressed as "atypical" or "unusual", have occasionally been reported. These terms do not represent specific clinicopathological findings, but include the cases that are not restricted to a single disease entity.[27,28] In addition, there are cases suspected to be associated with FTDP-17, such as the case reported by Henderson *et al.* that developed Pick's disease during the course of Parkinson's disease.[29] Some reported cases showed atypical locations of lesions, such as marked parietal lesions or the involvement of all cerebral lobes, as was observed in our case.[30-33]

The following cases of PDPB showed lesions involving all cerebral lobes. Elizabeth *et al.* reported a 69-year-old female with an 11-year entire course with a brainweight of 930 g.[31] Brain atrophy initially occured in the frontal and temporal lobes and subsequently involved all the cerebral cortices, but the superior temporal gyrus and calcarine cortex were relatively well preserved, and NFT were localized in the transentorhinal region. Pick bodies were observed in the neocortex of all the cerebral cortices, but there was no description of Pick bodies in the brain stem or spinal cord. Shibayama *et al.* reported a 64-year-old male with an entire course of 9 years and 8 months.[32] The initial symptoms were headaches and memory disturbance. Autopsy revealed a brainweight of 1180 g. Macroscopic examination showed severe atrophy localized in the temporal and frontal lobes, while histological examination showed neuronal loss beyond the macroscopically observed atrophy areas, extending to the parietal and occipital lobes, and ballooned neurons and Pick bodies in the entire cerebral cortex. Yoshimura reported a 66-year-old female showing an entire course of 15 years and a brainweight of 740 g.[33] In this case, Pick bodies were present in the red nucleus, dorsal motor nucleus of the vagus, and the uppermost cervical spinal cord, which have been reported as exceptional areas by Arima.[16]

In the reported cases, excluding ours, there was no description of remarkable clinical signs, such as bulging eyes and myoclonus. However, pathologically, all four cases, including ours, showed widespread distributions of Pick bodies not only in the frontal and temporal lobes, but also in the parietal and occipital lobes. In the case reported by Yoshimura, as well as ours, Pick bodies were widely distributed beyond the usual distribution areas, in which Pick bodies were observed in the brain stem and spinal cord. In the case reported by Elizabeth *et al.* and in ours, the calcarine cortex was relatively well preserved. The atypical clinical symptoms observed in our case and the neuropathologically uncommon findings mentioned above suggest that, in cases of PDPB with lesions involving all cerebral cortices, extensive lesions are probably present not only in the cerebral cortex, but also in the subcortical areas, and there is the possibility of manifesting neurological symptoms unseen in typical cases of PDPB.

REFERENCES

1. Pick A. Über die Beziehungen der senilen Hirnatrophie zur Aphasie. *Prag Med Wochenschr* 1892; **17**: 165–167.
2. Gans A. Betrachtungen über art und ausbreitung des krankhaften prozesses in einem fall von Pickscher atrophie des stirnhirns. *Ztschr ges Neurol Psychiat* 1922; **80**: 10–28.
3. Onari K, Spatz H. Anatomische Beiträge zur Lehre von Pickschen umschrieben Grobhirnrinden-Atrophie ('Picksche Krankheit'). *Z ges Neurol Psychiatr* 1926; **101**: 470–511.
4. Constantinidis J, Richard J, Tissot R. Histological and clinical correlations. *Eur Neurol* 1974; **11**: 208–217.
5. Knopman DS, Mastri AR, Frey WH, Sung JH, Rustan T. Dementia lacking distinctive histologic features: a common non-Alzheimer degenerative dementia. *Neurology* 1990; **40**: 251–256.
6. Oda T, Ikeda K, Akamatsu W *et al.* An autopsy case of corticobasal degeneration clinically misdiagnosed as Pick's disease (in Japanese with English abstract). *Seishin Shinkeigakuzasshi* 1995; **97**: 757–769.
7. Tsuchiya K, Ikeda K, Haga C *et al.* Atypical amyotrophic lateral sclerosisi with dementia mimicking frontal Pick's disease: a report of an autopsy case with a clinical course of 15 years. *Acta Neuropathol (Berl)* 2001; **101**: 625–630.
8. Kertesz A, Hudson L, Mackenzie IRA, Munoz DG. The pathology and nosology of primary progressive aphasia. *Neurology* 1994; **44**: 2065–2072.
9. The Lund and Manchester Groups. Clinical and neuropathological criteria for frontotemporal dementia. *J Neurol Neurosurg Psychiatry* 1994; **57**: 416–418.
10. Delacourte A, Sergeant N, Wattez A *et al.* Vulnerable neuronal subsets in Alzheimer's and Pick's disease are

distinguished by their isoform distribution and phosphorylation. *Ann Neurol* 1998; **43**: 193–204.
11. Uchihara T, Tsuchiya T. Pick body disease: a proposal. *Neuropathology* 2000; **20**: 246.
12. Togo T, Sahara N, Yen SH *et al.* Argyrophilic grain disease is a sporadic 4-repeat tauopathy. *J Neuropathol Exp Neurol* 2002; **61**: 537–556.
13. de Silva R, Lashley T, Gibb G *et al.* Pathological inclusion bodies in tauopathies contain distinct complements of tau with three or four microtubule-binding repeat domains as demonstrated by new specific monoclonal antibodies. *Neuropathol Appl Neurobiol* 2003; **29**: 288–302.
14. Arai T, Ikeda K, Akiyama H *et al.* Distinct isoforms of tau aggregated in neurons and glial cells in brains of patients with Pick's disease, corticobasal degeneration and progressive supranuclear palsy. *Acta Neuropathol (Berl)* 2001; **101**: 167–173.
15. Kosaka K, Matsushita M, Mehraein P. A clinicopathological study of Pick's disease – our sixty autopsied cases (in Japanese with English abstract). *Seishin Shinkeigakuzasshi* 1982; **84**: 101–113.
16. Arima K. Involvement of subcortical nuclei and brain stem in Pick's disease. A topographical study of Pick bodies. *Neuropathology* 1989; **9**: 105–115.
17. Cummings JL, Duchen LW. Klüver–Bucy syndrome in Pick disease: clinical and pathological correlation. *Neurology* 1981; **31**: 1415–1422.
18. Brown P, Rothwell P, Thompson TC *et al.* New observations on the normal auditory startle reflex in man. *Brain* 1991; **114**: 1891–1902.
19. Iwabuchi K, Kogure T, Oda T *et al.* Some problems on the clinical phenotype of Machado-Joseph disease in relation between their ages at onset (in Japanese with English abstract). *No Shinkei* 1993; **45**: 246–254.
20. Neary D, Snowden JS, Gustafson L *et al.* Frontotemporal lobar degeneration. A consensus on clinical diagnostic criteria. *Neurology* 1998; **51**: 1546–1554.
21. Hauser WA, Morris ML, Heston LL, Anderson VE. Seizures and myoclonus in patients with Alzheimer's disease. *Neurology* 1986; **36**: 1226–1230.
22. Risse SC, Lampe TH, Bird TD *et al.* Myoclonus, seizures, and paratonia in Alzheimer disease. *Alzheimer Dis Assoc Disord* 1990; **4**: 217–225.
23. Hattori H, Tanaka S, Kondoh H, Nishimura T, Hattori S. A case of juvenile Alzheimer's disease with various neurological features such as myoclonus, showing grumose degeneration in the dentate nucleus. *Clin Neurol* 1990; **30**: 647–653.
24. Fukutani Y, Cairns NJ, Everall IP, Chadwick A, Isaki K, Lantos PL. Cerebellar dentate nucleus in Alzheimer's disease with myoclonus. *Dement Geriatr Cogn Disord* 1999; **2**: 81–88.
25. Lüers T, Spatz H. Picksche Krankheit (progrssive umschriebene Grobhirnatrophie). In: Lubarsch O, Henke F, Rössle R (eds). *Handbuch der Spezielen Pathologischen Anatomie und Histologie*, Vol. 13/1A. Berlin, Heidelberg: Springer, 1957; 614–715.
26. Tsuchiya K, Ikeda M, Hasegawa K *et al.* Distribution of cerebral cortical lesions in Pick's disease with Pick bodies: a clinicopathological study of six autopsy cases showing unusual clinical presentations. *Acta Neuropathol* 2001; **102**: 553–571.
27. Horoupian DS, Dickson DW. Striatonigral degeneration, olivopontocerebellar atrophy and 'atypical' Pick disease. *Acta Neuropathol (Berl)* 1991; **81**: 287–295.
28. Arima K, Murayama S, Oyanagi S, Akashi T, Inose T. Presenile dementia with progressive supranuclear palsy tangles and Pick bodies: an unusual degenerative disorder involving the cerebral cortex, cerebral nuclei, and brain stem nuclei. *Acta Neuropathol (Berl)* 1992; **84**: 128–134.
29. Henderson JM, Gai WP, Hely MA, Reid WGJ, Walker GL, Halliday GM. Parkinson's disease with late Pick's dementia. *Mov Disord* 2001; **16**: 311–319.
30. Lang AE, Bergeron C, Pollanen MS *et al.* Parietal Pick's disease mimicking cortical-basal ganglionic degeneration. *Neurology* 1994; **44**: 1436–1440.
31. Elizabeth JC, Jacob HF, Elliot JM. Severe panencephalic Pick's disease with Alzheimer's disease-like neuropil threads and synaptophysin immunoreactivity. *Acta Neuropathol (Berl)* 1994; **88**: 479–484.
32. Shibayama H, Kitoh J, Marui Y, Kobayashi H, Iwase S, Kayukawa Y. An unusual case of Pick's disease. *Acta Neuropathol (Berl)* 1983; **59**: 79–87.
33. Yoshimura N. Topography of Pick body distribution in Pick's disease: a contribution to understanding the relationship between Pick's and Alzheimer's disease. *Clin Neuropathol* 1989; **8**: 1–5.

THE JOURNAL OF COMPARATIVE NEUROLOGY 505:352–362 (2007)

Chemical and Morphological Alterations of Spines Within the Hippocampus and Entorhinal Cortex Precede the Onset of Alzheimer's Disease Pathology in Double Knock-In Mice

CHIYE AOKI,[1]* VEERAVAN MAHADOMRONGKUL,[2] SHO FUJISAWA,[2] REBECCA HABERSAT,[3] AND TOMOAKI SHIRAO[4]

[1]Center for Neural Science, New York University, New York, New York 10003
[2]The Dominique D. Purpura Department of Neuroscience, Albert Einstein Medical College, Yeshiva University, Bronx, New York 10461
[3]Department of Psychology, Carthage College, Kenosha, Wisconsin 53140 [4]Department of Neurobiology and Behavior, Gunma University Graduate School of Medicine, Maebashi, Gunma 371-8511 Japan

ABSTRACT

Mice with knock-in of two mutations that affect beta amyloid processing and levels (2xKI) exhibit impaired spatial memory by 9–12 months of age, together with synaptic plasticity dysfunction in the hippocampus. The goal of this study was to identify changes in the molecular and structural characteristics of synapses that precede and thus could exert constraints upon cellular mechanisms underlying synaptic plasticity. Drebrin A is one protein reported to modulate spine sizes and trafficking of proteins to and from excitatory synapses. Thus, we examined levels of drebrin A within postsynaptic spines in the hippocampus and entorhinal cortex. Our electron microscopic immunocytochemical analyses reveal that, by 6 months, the proportion of hippocampal spines containing drebrin A is reduced and this change is accompanied by an increase in the mean size of spines and decreased density of spines. In the entorhinal cortex of 2xKI brains, we detected no decrement in the proportion of spines labeled for drebrin A and no significant change in spine density at 6 months, but rather a highly significant reduction in the level of drebrin A immunoreactivity within each spine. These changes are unlike those observed for the somatosensory cortex of 2xKI mice, in which synapse density and drebrin A immunoreactivity levels remain unchanged at 6 months and older. These results indicate that brains of 2xKI mice, like those of humans, exhibit regional differences of vulnerability, with the hippocampus exhibiting the first signatures of structural changes that, in turn, may underlie the emergent inability to update spatial memory in later months. J. Comp. Neurol. 505: 352–362, 2007.

Indexing terms: amyloid precursor protein; presenilin 1; drebrin; excitatory synapses; electron microscopic immunocytochemistry; ultrastructure

Acquisition, retention, and updating of memory rely on cellular mechanisms in the CNS that couple experience-evoked synaptic activities to modifications of synaptic strengths (Malinow and Malenka, 2002; Malenka and Bear, 2004). Conversely, there are strong indications that memory impairment associated with Alzheimer's disease (AD) is caused by the slow but progressive changes in synaptic physiology that precedes neuronal loss (Selkoe, 2002; Selkoe and Schenk, 2003). Recently, we showed that an animal model of AD exhibits reduced levels of AMPA receptors within hippocampal spines, together with deficits in spatial memory, impairments in synaptic physiology, and deposition of amyloid beta (Ab) plaques (Chang et al., 2006). The AD pathology, including the reduction of AMPA receptor subunits within postsynaptic spines of the

Grant sponsor: National Institutes of Health; Grant numbers: 1P30EY13079, R01-NS41091, and R01-EY13145 (all to C.A.); Grant sponsor: Research Challenge Fund of New York University (to C.A.).

*Correspondence to: Chiye Aoki, Center for Neural Science, New York University, 4 Washington Place, Rm 804, NY, NY 10003.
E-mail: chiye@cns.nyu.edu

Received 23 May 2007; Revised 6 June 2007; Accepted 1 August 2007
DOI 10.1002/cne.21485
Published online in Wiley InterScience (www.interscience.wiley.com).

hippocampus, is clearly evident by the 14th month, but some aspects of the pathology are likely to emerge several months earlier. We sought to identify constraints imposed upon synaptic plasticity at the onset of the disease. To this end, we looked for chemical and molecular changes within postsynaptic spines at ages preceding the emergence of synaptic and behavioral deficits associated with AD pathology.

The animal model of familial AD (FAD) we used in the previous study and again in this study was generated by targeted knock-in of two genes (2xKI)—one encoding the mutated amyloid precursor protein (APP; K670N/M671L, Swedish mutation with humanized amyloid beta sequence) and another encoding the mutated presenilin-1 (P264L; Flood et al., 2002). This gene-targeting technique ensures that the mutant genes' expressions are controlled by endogenous promoters and therefore are not overexpressed and also that the endogenous wildtype (WT) genes are absent. Accordingly, it has been shown that Ab plaques increase linearly, starting from 6 months (Chang et al., 2006). The same study has characterized the emergence and progression of the AD-like pathology in this 2xKI model. Based on this study, we now know that soluble forms of Ab (sAb, namely, sAb42 and sAb40) become detectable within brain homogenate supernatants by the second postnatal month and increase fourfold by 6–9 months. Deficiency in LTP expression does not become manifest until 7–9 months, whereas spatial memory deficits and reduction of AMPA receptor mEPSCs in the hippocampus are not measurable until 9–12 months. We reasoned that 6 months would be an ideal age for identifying synaptic changes, caused by the rise of sAb, that are beginning to impose constraints upon synaptic physiology.

A growing body of work indicates that synaptic plasticity is closely linked to structural changes in postsynaptic spines. Kasai et al. have shown that larger spines are morphologically stable, whereas smaller spines have a greater propensity to enlarge following LTP induction. Based on these observations, Kasai et al. suggest that the smaller spines are sites recruited for memory acquisition, whereas larger spines are sites for memory storage (Matsuzaki et al., 2001, 2004; Kasai et al., 2003). These ideas led us to hypothesize that synapses of the 2xKI mice may be impaired in the mechanism linking synaptic activity to structural changes in postsynaptic spines.

One protein proposed to be involved in the link between synaptic activity and spine morphology is an F-actin binding protein, drebrin (Shirao and Sekino, 2001; Shiraishi et al., 2003; Takahashi et al., 2003, 2005; Fujisawa et al., 2006; Kojima, 2007; Sekino et al., 2007). This protein is enriched at postsynaptic sides of excitatory synapses (Aoki et al., 2005). There are two isoforms of drebrin, drebrin E, which is expressed across multiple cell types from embryonic stages, and drebrin A, which is neuron specific and becomes the dominant isoform in adulthood. When drebrin A is expressed in non-neuronal cells, neurite-like processes appear (Shirao et al., 1992), whereas down-regulation of the drebrin A gene within hippocampal neurons grown in culture causes reduction in spine density, decreased width of spines, and suppression of the NMDA receptor targeting to spines (Takahashi et al., 2005). Drebrin (either the A or E isoform) is reduced within cortices and hippocampi of AD patients (Harigaya et al., 1996; Hatanpaa et al., 1999; Shim and Lubec, 2002; Calon et al., 2004) and begins to show regionally specific changes in levels at the stage at which patients are diagnosed with mild cognitive impairment (Counts et al., 2006). In the neocortex of rats and limbic cortex of mice, spines containing drebrin A are larger (Fujisawa et al., 2006; Kobayashi et al., 2007). These ideas and previous observations led us to predict that the loss of drebrin A may precede the deficits in spatial memory, impaired synaptic plasticity, and reduction in AMPA currents measurable in the hippocampus of 2xKI mice by 9 months. Thus, we compared the proportion of spines within samples of 2xKI brains that contain drebrin A with those of WT samples matched for brain region and age.

In brains of patients diagnosed with AD, degeneration and chemical changes occur earlier in the limbic cortex and the hippocampus, relative to the primary motor and primary sensory cortices (Braak and Braak, 1991; Counts et al., 2006). Our previous ultrastructural examination of the primary somatosensory cortex of 2xKI brains indicated that there are no signs of excitatory synapse loss or of decrement in drebrin A within spines, even at age 18 months or older (Mahadomrongkul, 2005). In this study, we analyzed the synaptic neuropil of the hippocampus, so that we could relate the ultrastructural data to the electrophysiological data previously collected from the hippocampus of 2xKI mice. In order to determine whether the cortex of FAD model mice also exhibits regional differences in pathology related to AD, we extended our analysis to the entorhinal cortex, one of the limbic areas of the cortex.

Our measurements in these two regions agree with our prediction regarding the spinous levels of drebrin A within 2xKI brains. We also observed subtle differences in the way drebrin A level and spine sizes change across the two brain regions. We discuss how these changes may lead to the reduction in activity-dependent fine-tuning of synaptic receptor levels and memory dysfunction.

Abbreviations

2xKI	double knock-in
Ab	amyloid beta
AD	Alzheimer's disease
AMPA	α-amino-3-hydroxy-5-methyl-4-isoxazolepropionic acid
APP	amyloid precursor protein
CNS	central nervous system
HRP-DAB	horseradish peroxidase-3,3'-diaminobenzidine HCl
LSD	least squares design
LTP	long-term potentiation
MCI	mild cognitive impairment
mEPSCs	miniature excitatory postsynaptic currents
NMDA	*N*-methyl-D-aspartate
sAb	soluble amyloid beta
PS1	presenilin 1
SIG	silver-intensified colloidal gold
WT	wildtype

MATERIALS AND METHODS

Animals

All the mice used in the experiment were male. The FAD mouse model used in this study were homozygous 2xKI mice expressing the genes for APP and presenilin-1 (PS1) carrying familial AD mutations (APP^{NLh} and $PS1^{P264L}$). For comparisons with WT mice, we used mice of identical background strain (129/CD-1). Cephalon

(West Chester, PA) generously provided us with the 2xKI mutant mice and the WT mice matched in age and background. The animals were housed for 1 day to >18 months at the New York University (NYU) animal facility. Before and after arrival at the facility, animals were maintained on a 12:12-hour light/dark cycle, fed ad libitum, and cared for according to the NIH *Guide for the Care and Use of Laboratory Animals* and also the guidelines approved by NYU's Animal Care and Use Committee.

We collected brain samples from three age groups. The number and ages of 2xKI mice were as follows: four aged 3–4 months, two aged 6 months, and three aged 18 months and older (>18 months). Two of the WT animals were 3–4 months old, two were 6 months old, and three were older than 18 months (>18 months). Brain samples from these six age-genotype groups were prepared by first anesthetizing the animals deeply with Nembutal (70 mg/kg) and then perfusing them transcardially with a mixture of 4% paraformaldehyde and 1% glutaraldehyde.

The drebrin A antibody

The rabbit anti-drebrin A antibody, DAS2, was generated against the peptide unique to the adult form of drebrin (residues 325–336) that is identical among mouse, rat, and human. This antibody was affinity-purified by the antigen peptide; it was previously shown by Western blotting to recognize a single band corresponding to drebrin A but not the band corresponding to the embryonic isoform, drebrin E (Aoki et al., 2005). Specific labeling of drebrin A within aldehyde-fixed tissue was demonstrated by elimination of immunoreactivity in rat brain tissue, when drebrin A was preadsorbed by the synthetic peptide used to generate the antiserum, and by the absence of immunolabeling when it was applied to brain tissue from drebrin A knock-out animals (Aoki et al., 2005).

Immunocytochemical detection of drebrin A and electron microscopy

Preparation of tissue. A Vibratome was used to prepare coronal sections of the hippocampus and entorhinal cortex at Bregma −2 mm, determined by the Franklin and Paxinos (2001) mouse atlas.

Details of tissue preparation for drebrin A immunocytochemistry and electron microscopy were exactly as described previously (Aoki et al., 2005; Mahadomrongkul, 2005). Two immunolabels were used: HRP-DAB, which allowed for optimal detection of drebrin A's presence within spines, and silver-intensified colloidal gold (SIG), which allowed for quantification of drebrin A levels within individual spines. Following the immunocytochemical steps, the HRP-DAB-labeled sections were postfixed by using osmium tetroxide and embedded by using Epon 812; the SIG-labeled sections were postfixed by using Phend's osmium-free method (Phend et al., 1995), so as to avoid the loss of SIG particles due to strong oxidation by osmium tetroxide. The SIG-labeled tissues were also embedded by using Epon 812.

Procedures for sampling postsynaptic spines. Ultrathin sections were collected from surface-most regions of Vibratome sections located in the stratum radiatum of the CA1 field of the hippocampus or layer 1 of entorhinal cortex. The stratum radiatum was the area chosen for this study, because this region in aged 2xKI mouse brains was shown in an earlier study to exhibit reduced immunoreactivity for AMPA receptors and AMPA receptor currents (Chang et al., 2006). There are four reasons we chose to analyze layer 1 of the entorhinal cortex. Axons and dendrites forming excitatory synapses are the most heterogeneous and of highest density here (Marin-Padilla, 1984), thereby allowing us to generalize our findings to excitatory synapses formed by multiple pathways most efficiently. Because excitatory synapses are formed the earliest in this layer and are maintained throughout development (Chun and Shatz, 1988), we reasoned that we would have the best chance of detecting cumulative effects of excitatory synaptic transmission here. Lastly, a preceding study of the somatosensory cortex of 2xKI mice analyzed layer 1 (Mahadomrongkul et al., 2005). We wanted to analyze a corresponding region of the entorhinal cortex, so that we could make comparisons between the two cortical regions most directly.

Images were captured by using a JEOL 1200EXII electron microscope (Peabody, MA) and a digital acquisition system from AMT (Danvers, MA) equipped with Hamamatsu's CCD camera (Bridgewater, NJ). The magnifications for capturing images were 40,000× for SIG-labeled tissue and 25,000× for the HRP-DAB-immunolabeled tissues. Spines were identified by the presence of asymmetric synapses, i.e., a thick postsynaptic density apposed to a profile identified as an axon terminal, based on the presence of multiple vesicles. The absence of mitochondria and microtubules served as additional cues to differentiate dendritic spines from dendritic shafts and mushroom spines.

Assessment of the proportion of spines containing drebrin A. For each age-genotype group, the proportion of spines containing drebrin A in the hippocampus was determined. This value was obtained in the following way. A minimum of 30 micrographs of the hippocampus was collected from samples of each brain that were immunolabeled for drebrin A, by using HRP-DAB as the marker. Each micrograph spanned 29 μm^2 of synaptic neuropil (i.e., gray matter that excludes cell bodies and blood vessels). For every group of 25 randomly encountered spines, the proportion containing HRP-DAB labeling was calculated. From these repeated measurements, the mean percent and SEM values were determined.

Analysis of the entorhinal cortex was restricted to the 6-month-old group. The proportion of spines containing drebrin A was assessed by using two sources of tissue: that immunolabeled by the HRP-DAB procedure and that immunolabeled by the SIG procedure. The analysis of spines labeled by the HRP-DAB procedure was identical to that described above for the hippocampus. For analysis of SIG-labeled tissue, a minimum of 35 digital images was captured, and the proportion of every group of 10 randomly encountered spines containing SIG labeling was calculated. From these repeated measurements, the mean percent and SEM values were determined.

Assessment of spine density in the synaptic neuropil. The same set of micrographs captured from the HRP-DAB-labeled tissue was used to calculate the density of drebrin A-labeled versus drebrin A-unlabeled spines per micrograph. For the analysis of spine density in the entorhinal cortex at 6 months of age, we also used tissue that had not undergone drebrin A immunolabeling.

Areas of spine profiles of the hippocampus and entorhinal cortex. These areas were also measured, by using the same set of micrographs from HRP-DAB-labeled

tissue used to determine spine density (per unit area), and Image J software (NIH).

Correlative assessment of spine profile area and drebrin A immunoreactivity level in the entorhinal cortex. To compare drebrin A levels within spines with spine size, we used a set of images captured from SIG-labeled tissue. The area, in nm^2, occupied by drebrin A-labeled and -unlabeled spines, all randomly encountered from the surface-most zone of Vibratome sections, was measured. The area occupied by all of the SIG particles within each spine cytoplasm was also measured, by using Image J.

Statistical analyses

All statistical analyses were performed by using the software Statistica (Statsoft, Tulsa, OK). When we were comparing data across the two genotypes, Student's t-test was used. When we were comparing multiple groups of data, one- or two-way ANOVA was performed, followed by post hoc Fisher's least squares design (LSD) test. Significance was accepted for $P < 0.05$. The Spearman rank order correlation analysis was performed to determine the degree of correlation between drebrin A immunoreactivity within spines (quantified as the area occupied by SIG particles) and spine area in the entorhinal cortex at the age of 6 months. Significance was accepted for $P < 0.05$.

Preparation of figures from electron microscopic digital images

The digital electron microscopic images, first captured by using a Hamamatsu CCD camera and software produced by AMT, were adjusted with Adobe Photoshop (version 7.0; Adobe Systems, San Jose, CA). Adjustments performed were for the purpose of matching the contrast and brightness of one digital image to another within a single figure. Adobe Photoshop was also used for cropping the image and for adding text and arrows. No dodging or copy-pasting of digital images was performed.

RESULTS

Morphological and chemical characteristics of spines in the hippocampus at 3, 6, and greater than 18 months

Drebrin A immunoreactivity in the hippocampus. In the hippocampus, the presence of drebrin A was assessed by using an anti-drebrin A antibody and HRP-DAB as the immunolabel. As was observed previously for regions elsewhere within mouse brains, drebrin A immunolabeling in both the WT and 2xKI hippocampi occurred within the cytoplasm of spines forming asymmetric, presumably excitatory synapses (Fig. 1A,B). Drebrin A immunolabeling also occurred in the dendritic shafts (e.g., Fig. 1A). Notably, for both the 2xKI and WT tissues, not all spines were immunoreactive for drebrin A. Thus, for each age and genotype, the proportion of postsynaptic spines in the CA1 field of the hippocampus exhibiting drebrin A immunolabeling was assessed. The outcome of the analysis revealed a significant main effect of genotype ($F(1,474) = 45.328$; $P < 0.0001$). The proportion of drebrin A-labeled spines was smaller for the 2xKI brains, compared with the WT brains (Fig. 1C). Post hoc Fisher's LSD analysis revealed that this difference across genotypes was most prevalent for the 6-month group ($P < 0.0001$). The proportion of drebrin A-containing spines in WT brains was less at ages 18 months and older (>18 months), compared with the values observed for the WT at 6 months of age. However, the difference across genotypes persisted at >18 months ($P < 0.001$). No difference was detected across the genotypes at 3 months.

Density of labeled and unlabeled spines in the hippocampus. A smaller proportion of drebrin A-immunoreactive synapses in the 2xKI hippocampus can result from an increase in spines lacking drebrin A and/or a decrease in the spines containing drebrin A. To identify and differentiate between these two contributing factors, we analyzed the density of labeled and unlabeled spines per unit area of synaptic neuropil separately. A genotype × immunoreactivity two-way ANOVA was performed for each age group. At 3 months, there was no significant difference in the density of spines, labeled or unlabeled, across the two genotypes (Fig. 1D; $F(1,356) = 1.75$; $P > 0.05$). In the 6-month group, there was a main effect of genotype ($F(1,236) = 22.31$; $P < 0.001$), showing a decrease in synapse density for the 2xKI tissue relative to that of age-matched WT tissue. This difference across genotypes was due to a decrease in the density of drebrin A-labeled spines within the 2xKI brains (−56%, $P < 0.001$, Fisher's LSD) and a concomitant increase in the density of unlabeled spines in the same synaptic neuropil, which also was significant (+54%, $P < 0.001$, Fisher's LSD). In comparison, the older group (>18 months) showed less difference in the density of spines across genotypes, even though the difference was statistically significant ($F(1,356) = 4.86$; $P < 0.05$), and the change was in the opposite direction (greater synapse density in the 2xKI neuropil, compared with the WT neuropil). The increased synapse density in 2xKI tissue was brought about by the increase in the density of drebrin-negative spines (+32%, $P < 0.0001$).

For comparisons of the density of labeled spines across ages, one-way ANOVA with age-genotype condition as the independent factor was performed. This test verified an interaction of age-genotype upon the density of labeled spines ($F(5,474) = 47.39$; $P < 0.0001$). Post hoc analysis using Fisher's LSD showed a 117% difference for the WT animals between 3 and 6 months ($P < 0.001$), reflecting an increase as the animal continues to mature (Fig. 1D). This chronological pattern was greatly reduced among the 2xKI brains, which showed only a small (17%) increase from 3 to 6 months, a magnitude that did not reach statistical significance ($P = 0.14$). The densities of labeled spines in the synaptic neuropil of 2xKI hippocampi at 6 months were already like those observed for the >18-month neuropil of the WT and 2xKI genotypes ($P = 0.73$ and 0.71, respectively), indicating signs of accelerated degeneration or failure to thrive from 3 to 6 months.

Areas of spine profiles in the hippocampus. Assessment of synapse density from two-dimensional (2D) images can be influenced by the sizes of the spines and synapses, because larger spines are captured more readily in single ultrathin sections (Mouton, 2002). We wondered whether the lower rate of encounter with drebrin A-immunoreactive spines within the 6-month 2xKI hippocampus might be due to spine size reduction. This possibility was tested by measuring the area occupied by each spine profile encountered within the same neuropil (i.e., same set of micrographs) used to assess synapse density. This analysis revealed a difference in spine profile area across genotypes for the 6-month group ($t = -3.56$; $P <$

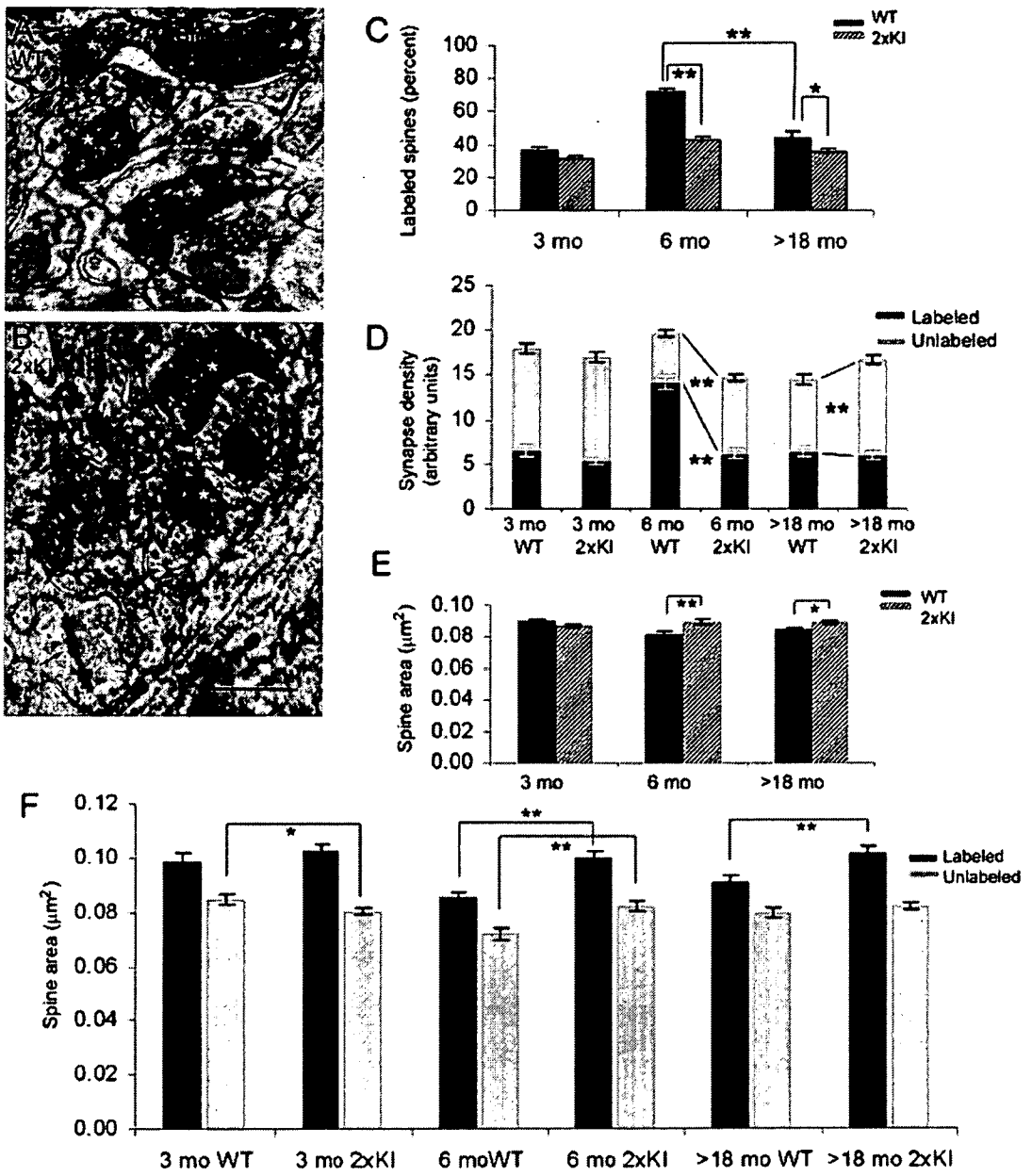

Fig. 1. Dendritic spines of the hippocampus immunolabeled for drebrin A. **A,B:** Examples of digitally captured electron micrographs from the stratum radiatum of the CA1 of a WT and a 2xKI mouse, respectively, at the age of 6 months. The tissues were processed to immunolabel for drebrin A, by using HRP-DAB as the electron-dense tag. Asterisks indicate examples of spines that are immunolabeled for drebrin A, and arrows point to unlabeled spines. Sh, example of a dendritic shaft that is contiguous with the labeled spine and is also immunoreactive. **C:** The proportion of synapses labeled for drebrin A is markedly different at 6 months. The synapses encountered from each age-genotype were divided into multiple groups (at least 60), each consisting of 25 synapses. For each group, the proportion of synapses immunolabeled for drebrin was determined. The graph shows the mean and SEM values of the percent labeled. **, $P < 0.0001$; *, $P < 0.001$ (two-way ANOVA). **D:** Spine density difference across genotypes is most prevalent at 6 months. The same sets of synapses analyzed in C were subjected to synapse density measurements. The number of labeled and unlabeled synapses appearing in each micrograph equal to 29 μm^2 (arbitrary unit) was determined. The graph represents the mean and SEM values obtained per age-genotype (minimum of 60 micrographs). The dark bars represent the density of labeled synapses per unit area, and the light bars represent the unlabeled synapses per unit area. **, $P < 0.0001$. **E:** The areas of spines differ the most at 6 months. The same sets of synapses analyzed for data shown in C and D were subjected to spine profile area comparisons across genotypes. The solid bars represent the mean values of spines in the WT brains, and the striped bars represent the mean values of spine sizes in the 2xKI brains. **, $P < 0.0001$; *, $P < 0.05$. **F:** Both the labeled and unlabeled spines are larger in the hippocampus of 2xKI mice at 6 months. The same sets of synapses analyzed in C–E were first categorized as labeled or unlabeled spines and then subjected to area comparisons across genotypes. Both the labeled and unlabeled spines exhibit size differences at 6 months. ($P < 0.0001$). At >18 months, only the drebrin A-labeled spines are larger in the hippocampus of 2xKI mice ($P < 0.0001$). At 3 months, the unlabeled spines of 2xKI hippocampi are slightly smaller ($P < 0.05$). The numbers of observations were 1,078 and 2,042 for 3-month WT and 2xKI mice, respectively; 1,177 and 879 for 6-month WT and 2xKI; and 1,306 and 1,507 for >18-month WT and 2xKI mice. For abbreviations, see list. Scale bar = 500 nm in B (applies to A,B).

0.0001) and a less marked, although still significant difference in the >18-month group ($t = -2.30$; $P < 0.05$). However, the reduced density of spines in the 2xKI tissue could not be due to reduction of spine sizes, because for both age groups, the spine profile area was relatively larger within the 2xKI neuropil than within the WT neuropil (Fig. 1E). These findings indicated that the decreased encounter with spines in the 6-month 2xKI neuropil, relative to the 6-month WT neuropil, did reflect a reduction in spine density rather than an increased failure to detect spine profiles. No difference was detectable across the genotypes of the 3-month group.

Area of spines containing and lacking drebrin A. The observed difference in the size of spines was an unexpected result. Earlier work on the cortex had shown that spines containing drebrin A are, on average, larger than those lacking drebrin A (Fujisawa et al., 2006; Kobayashi et al., 2007). Based on the observation that drebrin A-containing spines were less numerous in the hippocampus of 2xKI mice, we had predicted that spines contained within these tissues would be smaller. In order to determine whether there might be a reduction in the size of spines specific to those lacking drebrin A, we next examined areas of drebrin A-labeled and drebrin A-unlabeled spines separately (Fig. 1F). We first confirmed earlier observations, namely, that for each age-genotype group, the drebrin A-immunoreactive spines are larger than the spines lacking drebrin A immunoreactivity (two-way ANOVA, ($F(1,5) = 183.75$; $P < 0.0001$). More importantly, post hoc analysis using Fisher's LSD showed that in the 6-month 2xKI neuropil, both drebrin A-immunoreactive and -negative spines were larger than those in the 6-month WT neuropil ($P < 0.0001$ for both). Such differences in spine size across genotypes were also observed for the drebrin A-immunoreactive spines of the >18-month group ($P < 0.0001$). In contrast, the 3-month group of the 2xKI hippocampus showed a significant but relatively smaller decrease in the area of unlabeled (but not the labeled) spines, relative to those of WT hippocampus ($P < 0.05$ for the unlabeled group of spines). Together, these observations indicated that spines of both varieties—those with and those without drebrin A—began to exhibit subtle differences in the synaptic neuropil by 6 months, with the 2xKI hippocampi containing fewer but larger spines.

Morphological and chemical characteristics in the 6-month entorhinal cortex

All of the analyses described above pointed to 6 months as the approximate age at which the effect of double knock-in begin to emerge. To address whether these changes are also evident in the entorhinal cortex by 6 months, we first assessed whether spines in the entorhinal cortex contain drebrin A. Electron microscopic visualization of the entorhinal cortex at 6 months revealed robust drebrin A labeling within spines and dendritic shafts of both the WT and 2xKI brains (Fig. 2A,B). Thus, we proceeded with analyses of spine density, spine size, and drebrin A immunoreactivity within postsynaptic spines.

Spine density in the entorhinal cortex. Ultrastructural analysis of spine density was performed as described for the hippocampus, by using two sources of Vibratome sections; one set had undergone drebrin A immunocytochemistry, and a second set was not immunolabeled. Regardless of the tissue source, the entorhinal cortex exhibited no difference in the density of spines across the two genotypes at 6 months ($t = 1.09$; $P > 0.05$ for tissue that had not undergone drebrin A immunocytochemistry [Fig. 2C]; $t = -0.001$; $P > 0.05$, for tissue that had undergone drebrin A immunocytochemistry).

Drebrin A immunoreactivity within spines of the entorhinal cortex. For the analysis of the proportion of spines containing drebrin A, we first used HRP-DAB as the immunolabel, so as to optimize detection of drebrin A. We detected no difference in the percent of spines immunolabeled for drebrin A (Fig. 2D, $t = 0.21$; $P > 0.05$). This assessment was confirmed by using SIG as the label ($t = 1.35$; $P > 0.05$ [Fig. 2E]). As was observed for the hippocampus of both the WT and 2xKI brains, the spines of the entorhinal cortex of both genotypes containing drebrin A were consistently larger than those lacking drebrin A, whether we used SIG (Fig. 2G, main effect for drebrin A labeling, $F(1,347) = 54.31$; $P < 0.0001$) or HRP-DAB ($F(1, 855) = 31.395$; $P < 0.0001$) as the immunolabel. However, unlike the hippocampus, the mean area of drebrin A-immunoreactive spines of entorhinal cortex from 2xKI brains was not significantly different from the that of the labeled spines of the WT brains, whether we used SIG or HRP-DAB to detect drebrin A ($P > 0.05$, Fisher's LSD).

Drebrin A immunoreactivity within spines of the entorhinal cortex. We used SIG area to quantify the relative level of drebrin A immunoreactivity within individual spines. For both genotypes, drebrin A immunoreactivity within spines varied by more than 40-fold. Specifically, the SIG area occupying the spine cytoplasm ranged from 187 nm^2 to 87,282 nm^2. We detected a large difference across genotypes in drebrin A immunoreactivity within the labeled spines (Fig. 2F, $t = 3.46$; $P < 0.001$, Student's t-test). Analysis of the frequency of spines containing varying levels of drebrin A immunoreactivity indicated that the differences in drebrin A immunoreactivity across the genotypes was due to a shift in the population of spines from the ones with extremely high levels of drebrin A immunoreactivity (>12,000 nm^2 within a single spine) to those with lower levels of drebrin A immunoreactivity (<6,000 nm^2; Fig. 3A1,A2). The entorhinal cortex of both genotypes exhibited wide variation in spine profile areas as well as drebrin A immunoreactivity (Fig. 3B). These two parameters were positively correlated for both WT and 2xKI ($r = 0.5249$ and 0.4071, respectively; $P < 0.05$ for both).

DISCUSSION

Our previous studies of 2xKI mice indicated that their inability to update spatial memory becomes evident at around 9–12 months, whereas the earliest signs of decrement in synaptic plasticity are detectable around 7–8 months (Chang et al., 2006). This study sought to determine whether these decrements in synaptic and behavioral plasticity may be dictated by limitations in the synaptic structure within two brain regions recognized to be of particular importance for learning and memory—the hippocampus and the entorhinal cortex. By 6 months, changes in the levels of drebrin A immunoreactivity (and presumably of drebrin A protein levels) become detectable specifically within postsynaptic spines of these two brain regions. The significance of these changes is discussed below.

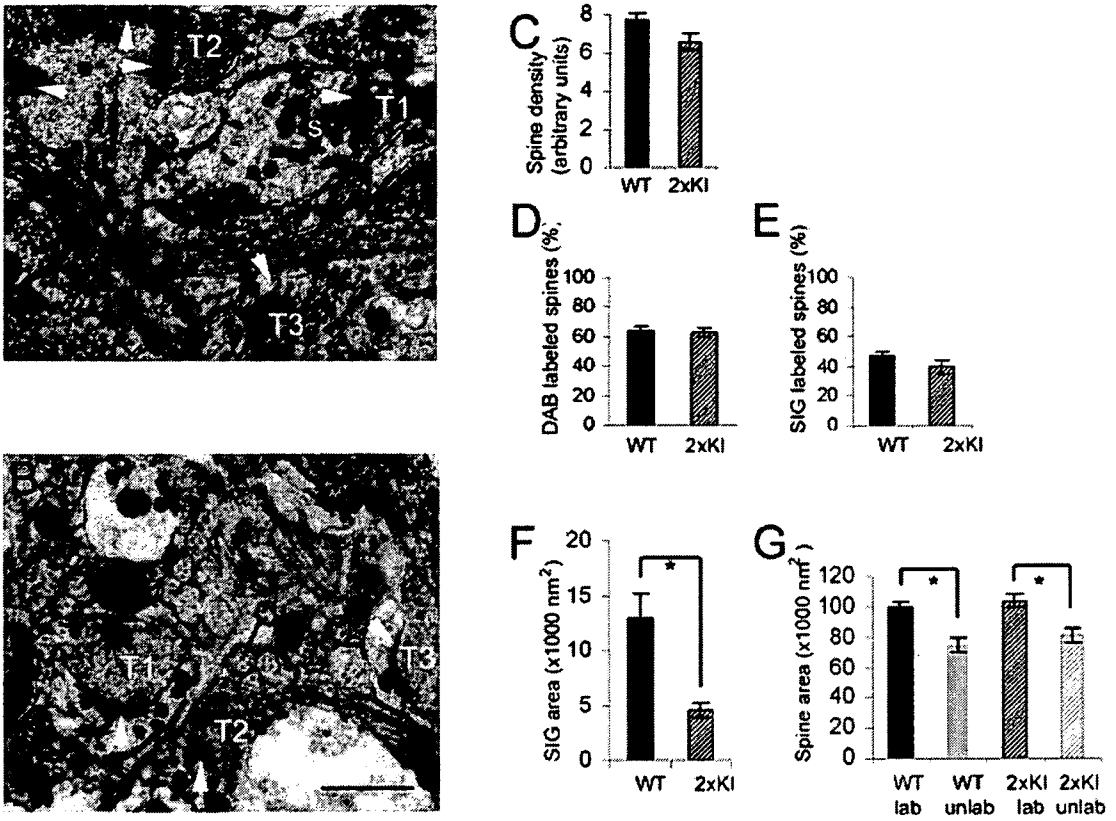

Fig. 2. At 6 months, spines of the WT entorhinal cortex contain greater amounts of drebrin A immunoreactivity compared with 2xKI spines. **A,B:** Examples of spine labeling in layer 1 of the entorhinal cortex of a WT and a 2xKI animal, respectively. The large maximally electron-dense particles, such as the one tagged with a white letter s in A, represent silver-intensified gold (SIG) immunolabeling for drebrin A. White arrows point to the postsynaptic densities (PSD). T1, T2, and T3 are presynaptic axon terminals. **C:** Mean and SEM values of the number of postsynaptic spines per unit area (spine density). The samples were taken from Vibratome sections that were semiadjacent to the ones shown in A and B. These tissues were not immunolabeled for drebrin A and were postfixed by using the osmium procedure. Altogether, 514 spines from WT tissue and 484 spines from 2xKI tissue were encountered within fields of equal total area (30 micrographs × 29 μm^2 per micrograph shot at a magnification of 25,000× = 870 μm^2) for each animal. We detected no difference across the genotypes ($t = 1.09$, $P > 0.05$). **D:** Mean and SEM values of the proportion of spines encountered from tissue that underwent drebrin A immunolabeling by the HRP-DAB procedure. For each animal, a minimum of 30 micrographs at a magnification of 25,000×were captured to sample 15–17 groups of 25 spines (375 spines per animal), for assessing the proportion of spines immunolabeled for drebrin A. We detected no difference across the genotypes ($t = 0.21$, $P > 0.05$). **E–G:** Mean and SEM values of three types of measurements made from Vibratome sections that underwent the SIG immunolabeling procedure to detect drebrin A. **E:** Proportion of postsynaptic spines with drebrin A immunoreactivity. Sixteen groups of 10 synapses were sampled from the WT tissue, and 17 groups of 10 synapses were sampled from the 2xKI tissue. **F:** Mean and SEM values of area occupied by SIG particles within each labeled spine encountered. **G:** Cytoplasmic area captured within individual spine profiles within single 2D images that were labeled and unlabeled. Asterisks indicate statistical significance ($P < 0.001$) by Student's t-test in F and two-way ANOVA in G. For abbreviations, see list. Scale bar = 500 nm in B (applies to A,B).

Regional differences in drebrin A distribution among spines

Although both the hippocampus and entorhinal cortex exhibit lower levels of drebrin A immunoreactivity within spines of 2xKI animals relative to those of age-matched WT animals, closer inspection by using an electron microscope revealed that the two regions differ subtly in their pattern of drebrin A decrement. In the hippocampus, the decrease of drebrin A manifested as a decrease in the proportion of spines that are drebrin A immunoreactive. In contrast, the entorhinal cortex showed no detectable difference in the proportion of spines immunoreactive for drebrin A. However, the use of discrete silver-intensified gold particles (SIG) allowed us to detect lower levels of drebrin A immunoreactivity within individual spines. The more subtle differences across the genotypes in the entorhinal cortex at 6 months suggest that the change in spinous drebrin A emerges first as a decline (or a failure to increase in level) but not a complete loss. In the hippocampus, the loss of drebrin A may be more drastic, leading to the emergence of spines that have become "emptied" of drebrin A to a level that is undetectable, even by the most sensitive labeling method currently available for immunodetection, i.e., the avidin-biotin complex with HRP-DAB as the tag. The increased density of unlabeled spines that we measured for the hippocampus from 3 to 6 months

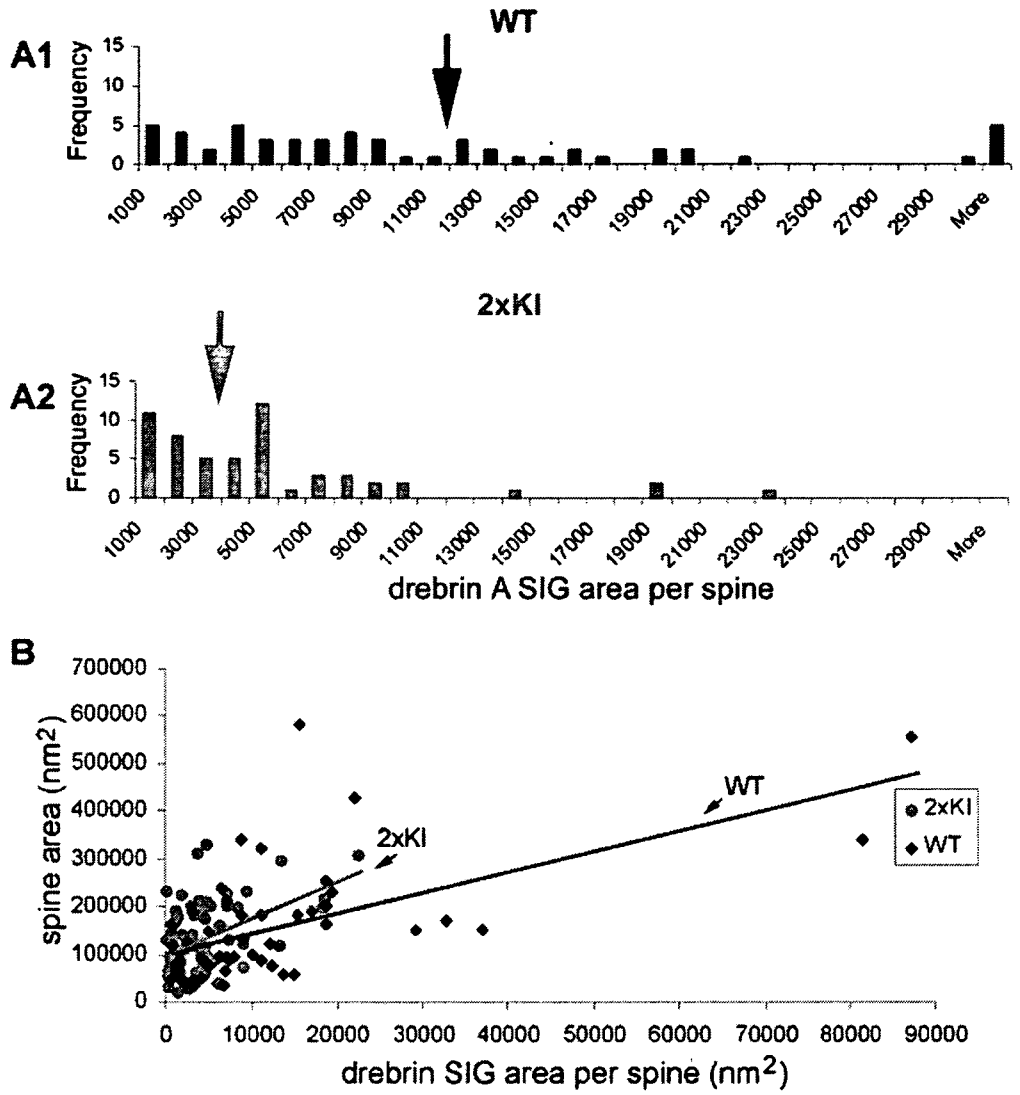

Fig. 3. Spines with low levels of drebrin A immunoreactivity are more numerous in the entorhinal cortex of 2xKI brains. SIG immunolabeling for drebrin A indicates that the levels of drebrin A can vary by more than 40-fold. **A1,A2:** Outcome of a frequency analysis performed to compare the relative number of spines containing varying levels of drebrin A immunoreactivity. Levels of drebrin A within spines was quantified by measuring the area occupied by SIG particles, using Image J software. This analysis indicates that, in the 2xKI entorhinal cortex, spines containing low levels of drebrin A immunoreactivity are more numerous than those containing high levels of drebrin A immunoreactivity. In contrast, the entorhinal cortices of WT brains contain a more even distribution of spines across the range of drebrin A immunoreactivity. **B:** Drebrin A immunoreactivity correlates weakly with dendritic spine size ($r = 0.524887$ for WT, 0.407118 for 2xKI, $P < 0.05$). [Color figure can be viewed in the online issue, which is available at www.interscience.wiley.com.]

supports this idea. The lower density of labeled spines in the 2xKI hippocampus suggests that spines are not only losing drebrin A but may be disappearing altogether. Alternatively, it is possible that sAb is beginning to have its effect as early as 3 months, by suppressing the program that normally increases spines with drebrin A between 3 and 6 months. Future studies that correlate drebrin A level to the half-life and motility of spines would be able to test whether drebrin A contributes to the structural stability of spines.

The SIG-based labeling procedure that we used for the entorhinal cortex revealed that the reduction in the average level of drebrin A within spines of 2xKI mice reflects the loss of spines with extremely high levels of drebrin A (i.e., more than 40-fold above the threshold level for detection) and a concomitant increase in the number of smaller spines with lower levels of drebrin A. The results obtained from spine density measurements of the entorhinal cortex indicate that spines here are unlike those in the hippocampus in that they are not yet disappearing. However, it is possible that these spines are exhibiting signs that lead to their disappearance as the animal attains the age at which the inability to update spatial memory becomes apparent. As was proposed for the hippocampus, it

is possible that sAb is beginning to manifest its effect in the entorhinal cortex by 3 months by suppressing the normal program to increase drebrin A level within individual spines.

Although both the hippocampus and entorhinal cortex of 2xKI mice exhibit decreases of drebrin A within spinous portions of dendrites by 6 months, this is not the pattern observed globally. In our hands, the somatosensory cortex at 6 months shows no decrease in the density of spines containing drebrin A or of the levels of drebrin A immunoreactivity within individual spines (Mahadomrongkul, 2005). Such differences across brain regions in drebrin A levels were noted recently by Counts et al. (2006), who compared drebrin A levels across brain regions of patients diagnosed with mild cognitive impairment (MCI) as well as at the end stages of AD. Previous studies have also noted that limbic areas are prone to earlier and more severe degeneration, when compared with the somatosensory and motor regions of cortex (Braak and Braak, 1991). Our analysis of the 2xKI model indicates that the changes in drebrin A levels that were measured previously from homogenates relate to levels that are specific to postsynaptic spines and can predate the loss of spines.

It is not yet known why some regions degenerate more or earlier than others, but one hypothesis is that the culprit of the disease—sAb—binds to and then accumulates near nicotinic acetylcholine receptors containing the $\alpha 7$ subunits, which are more abundant in the limbic cortex and hippocampus than other cortical regions (D'Andrea and Nagele, 2006). It is possible that, even in the healthy stage, these receptors tend to occur near excitatory synapses more often within the limbic cortex and hippocampus, relative to regions that are spared degeneration until later ages. An electron microscopic immunocytochemical study that systematically compares the localization of nicotinic receptors in relation to excitatory synapses across the brain regions would be one way to test the validity of this idea. It would also be important to learn whether sAb occurs extracellularly or intracellularly.

The hippocampus but not the cortex exhibits changes in spine size

Although smaller profile sizes can cause underestimation in the counting of profiles (Mouton, 2002), the decreased density of spines we observed within the neuropil of 2xKI hippocampi cannot be explained by a reduction in spine sizes. On the contrary, the mean spine size was greater for the 2xKI hippocampi, when compared with age-matched WT hippocampi.

A number of studies, including ours, have documented a trend that is the opposite of what we have just described here. Specifically, what had been observed previously is that spines containing drebrin A tend to be larger. For example, the overexpression of drebrin A within cultured neurons causes spines to become unusually large (Hayashi and Shirao, 1999). Ultrastructural analysis of the rat somatosensory cortex and mouse entorhinal cortex also showed that spines containing drebrin A are, on average, larger than those without (Fujisawa et al., 2006; Kobayashi et al., 2007). Our current observation agrees, in part, with these previous studies, because we observed a weak correlation between drebrin A levels and spine sizes (in the entorhinal cortex), and the average areas of spines containing drebrin A were greater than those without (for both regions). Thus, what we observed for the 2xKI hippocampus, namely, a reduced proportion of spines with drebrin A, accompanied by an increase in the average area of individual spine profiles, was contrary to our expectation. Moreover, the prevalence of larger spine sizes was detected for spines lacking drebrin A as well as those containing drebrin A. These patterns indicate that, in adult hippocampus, drebrin A level influences but does not dictate spine size.

What might be the factor(s) influencing spine sizes? One possibility is sAb, whose presence becomes detectable within homogenates of 2xKI brains by 2 months and will have risen fourfold by 6–9 months. However, a recent in vitro study reports on a decrease (not an increase) in the size of dendritic spine, following exposure of hippocampal neurons to picomolar concentrations of sAb for 1–2 hours (Calabrese et al., 2007; Shankar et al., 2007). The same study also reports on this decrease being transient: another and perhaps opposite response might be expected following chronic exposure to sAb, as the sAb causes desensitization of nicotinic receptors containing $\alpha 7$ subunits.

Besides this link of drebrin A to spine size, drebrin A has also been proposed to play a role in regulating the trafficking of synaptic molecules. Downregulation of drebrin A within cultured hippocampal neurons leads to the loss of activity-dependent trafficking of NMDAR subunits into spines (Takahashi et al., 2005). Conversely, an acute pharmacological manipulation that induces an increase of NR2A subunits into spines (Aoki et al., 2003) also leads to an increase in the proportion of spines containing drebrin A, without inducing measurable increases in spine size or lengths of postsynaptic densities (Aoki et al., 2003; Fujisawa et al., 2006). Studies that determine the robustness of activity-dependent trafficking of synaptic molecules within spines of 2xKI mice with decreased levels of drebrin A would be helpful for testing this idea.

Measurement of the area of individual spine profiles also had the utility of allowing us to speculate about the abundance of glutamate receptors within spines. Earlier results obtained from electron microscopic immunocytochemistry have shown that the diameter of the active zone of axospinous junctions correlates well with the abundance of AMPA type of glutamate receptors (Matsubara et al., 1996; Kharazia and Weinberg, 1999; Matsuzaki et al., 2001). Within in vitro slices, synapse strengthening that follows LTP induction is achieved by an increased delivery of AMPA receptor subunits to the synaptic membrane (Shi et al., 1999; Rumpel et al., 2005), and this change is accompanied by increased volume of spines (Matsuzaki et al., 2004; Park et al., 2006). It has been noted that smaller spines are more amenable to LTP and spine enlargement, whereas larger spines are morphologically more stable (Trachtenberg et al., 2002; Matsuzaki et al., 2004; Zuo et al., 2005). When these observations have been put together (for review, see Hayashi and Majewska, 2005; Segal, 2005), it has been hypothesized that larger spines are sites for memory storage, whereas smaller spines are sites for acquisition of new memory (Kasai et al., 2003).

Prompted by these ideas, we reasoned that the cumulative, activity-dependent modifications of synaptic strengths may be reflected in the size of individual postsynaptic spine profiles that we measured from 2D images of spines. The relative scarcity in the number of small spines in the hippocampus of 2xKI mice indicates that fewer of their synapses may be available to become engaged in the formation of new, labile memory. Synapse

density in the hippocampus of 2xKI mice at 6 months is lower than the densities observed in age-matched WT hippocampi and is similar to that observed by 18 months in both genotypes. Similarly, the average size of spines that we observed for the hippocampus of 2xKI mice at 6 months is greater than that of age-matched WT hippocampi but is similar to those of the 18-month hippocampi of both genotypes. What we have observed in the 2xKI hippocampi at 6 months may be the cellular signatures and structural constraints that are accelerated by the presence of sAb, leading to excessive stability of spines and the animals' inability to update spatial memory, as was noted from the behavioral tests of the 2xKI mice (Chang et al., 2006), other animal models of FAD (Moolman et al., 2004; Trinchese et al., 2004; Ryman and Lamb, 2006; Shen and Kelleher, 2007), and AD patients (Braak and Braak, 1991; Selkoe, 2002).

ACKNOWLEDGMENTS

We thank Cephalon (West Chester, PA) for providing us with the 2xKI mutant mice and the WT mice matched in age and background. We thank Hilda Pena Fernandez for her technical assistance and intellectual input in the data analyses.

LITERATURE CITED

Aoki C, Fujisawa S, Mahadomrongkul V, Shah PJ, Nader K, Erisir A. 2003. NMDA receptor blockade in intact adult cortex increases trafficking of NR2A subunits into spines, postsynaptic densities, and axon terminals. Brain Res 963:139—149.

Aoki C, Sekino Y, Hanamura K, Fujisawa S, Mahadomrongkul V, Ren Y, Shirao T. 2005. Drebrin A is a postsynaptic protein that localizes in vivo to the submembranous surface of dendritic sites forming excitatory synapses. J Comp Neurol 483:383–402.

Braak H, Braak E. 1991. Neuropathological stageing of Alzheimer-related changes. Acta Neuropathol (Berl) 82:239–259.

Calabrese B, Shaked GM, Tabarean IV, Braga J, Koo EH, Halpain S. 2007. Rapid, concurrent alterations in pre- and postsynaptic structure induced by naturally-secreted amyloid-beta protein. Mol Cell Neurosci 35:183–193.

Calon F, Lim GP, Yang F, Morihara T, Teter B, Ubeda O, Rostaing P, Triller A, Salem N Jr, Ashe KH, Frautschy SA, Cole GM. 2004. Docosahexaenoic acid protects from dendritic pathology in an Alzheimer's disease mouse model. Neuron 43:633–645.

Chang EH, Savage MJ, Flood DG, Thomas JM, Levy RB, Mahadomrongkul V, Shirao T, Aoki C, Huerta PT. 2006. AMPA receptor downscaling at the onset of Alzheimer's disease pathology in double knockin mice. Proc Natl Acad Sci U S A 103:3410–3415.

Chun JJ, Shatz CJ. 1988. Redistribution of synaptic vesicle antigens is correlated with the disappearance of a transient synaptic zone in the developing cerebral cortex. Neuron 1:297–310.

Counts SE, Nadeem M, Lad SP, Wuu J, Mufson EJ. 2006. Differential expression of synaptic proteins in the frontal and temporal cortex of elderly subjects with mild cognitive impairment. J Neuropathol Exp Neurol 65:592–601.

D'Andrea MR, Nagele RG. 2006. Targeting the alpha 7 nicotinic acetylcholine receptor to reduce amyloid accumulation in Alzheimer's disease pyramidal neurons. Curr Pharm Des 12:677–684.

Flood DG, Reaume AG, Dorfman KS, Lin YG, Lang DM, Trusko SP, Savage MJ, Annaert WG, De Strooper B, Siman R, Scott RW. 2002. FAD mutant PS-1 gene-targeted mice: increased A beta 42 and A beta deposition without APP overproduction. Neurobiol Aging 23:335–348.

Franklin KBJ, Paxinos G. 1996. The mouse brain in stereotaxic coordinates. Academic Press.

Fujisawa S, Shirao T, Aoki C. 2006. In vivo, competitive blockade of N-methyl-D-aspartate receptors induces rapid changes in filamentous actin and drebrin A distributions within dendritic spines of adult rat cortex. Neuroscience 140:1177–1187.

Harigaya Y, Shoji M, Shirao T, Hirai S. 1996. Disappearance of actin-binding protein, drebrin, from hippocampal synapses in Alzheimer's disease. J Neurosci Res 43:87–92.

Hatanpaa K, Isaacs KR, Shirao T, Brady DR, Rapoport SI. 1999. Loss of proteins regulating synaptic plasticity in normal aging of the human brain and in Alzheimer disease. J Neuropathol Exp Neurol 58:637–643.

Hayashi K, Shirao T. 1999. Change in the shape of dendritic spines caused by overexpression of drebrin in cultured cortical neurons. J Neurosci 19:3918–3925.

Hayashi Y, Majewska AK. 2005. Dendritic spine geometry: functional implication and regulation. Neuron 46:529–532.

Kasai H, Matsuzaki M, Noguchi J, Yasumatsu N, Nakahara H. 2003. Structure-stability-function relationships of dendritic spines. Trends Neurosci 26:360–368.

Kharazia VN, Weinberg RJ. 1999. Immunogold localization of AMPA and NMDA receptors in somatic sensory cortex of albino rat. J Comp Neurol 412:292–302.

Kobayashi CA, Aoki C, Kojima N,Yamazaki H, Shirao T. 2007. Drebrin A content correlates with spine head size in the adult mouse cerebral cortex. J Comp Neurol 503:618–26.

Kojima NaS, T. 2007. Synaptic dysfunction and disruption of postsynaptic drebrin-actin complex: a study of neurological disorders accompanied by cognitive deficits. J Neurosci Res 58:1–5.

Mahadomrongkul V, Huerta, P.T., Shirao, T. and Aoki, C. 2005. Altered distribution of drebrin A in spines of sensory cortex layer I of mice expressing mutated APP and PS1 genes. Brain Res 1064:66–74.

Malenka RC, Bear MF. 2004. LTP and LTD: an embarrassment of riches. Neuron 44:5–21.

Malinow R, Malenka RC. 2002. AMPA receptor trafficking and synaptic plasticity. Annu Rev Neurosci 25:103–126.

Marin-Padilla M. 1984. Neurons of layer I: a developmental analysis. In: Peters A, Jones EG, editors. Cerebral cortex, vol. 1: Cellular components of the cerebral cortex. New York: Plenum. p 447–478.

Matsubara A, Laake JH, Davanger S, Usami S, Ottersen OP. 1996. Organization of AMPA receptor subunits at a glutamate synapse: a quantitative immunogold analysis of hair cell synapses in the rat organ of Corti. J Neurosci 16:4457–4467.

Matsuzaki M, Ellis-Davies GC, Nemoto T, Miyashita Y, Iino M, Kasai H. 2001. Dendritic spine geometry is critical for AMPA receptor expression in hippocampal CA1 pyramidal neurons. Nat Neurosci 4:1086–1092.

Matsuzaki M, Honkura N, Ellis-Davies GC, Kasai H. 2004. Structural basis of long-term potentiation in single dendritic spines. Nature 429: 761–766.

Moolman DL, Vitolo OV, Vonsattel JP, Shelanski ML. 2004. Dendrite and dendritic spine alterations in Alzheimer models. J Neurocytol 33:377–387.

Mouton PR. 2002. Principles and practices of unbiased stereology: an introduction for bioscientists. Baltimore: The Johns Hopkins University Press.

Park M, Salgado JM, Ostroff L, Helton TD, Robinson CG, Harris KM, Ehlers MD. 2006. Plasticity-induced growth of dendritic spines by exocytic trafficking from recycling endosomes. Neuron 52:817–830.

Phend KD, Rustioni A, Weinberg RJ. 1995. An osmium-free method of Epon embedment that preserves both ultrastructure and antigenicity for post-embedding immunocytochemistry. J Histochem Cytochem 43: 283–292.

Rumpel S, LeDoux J, Zador A, Malinow R. 2005. Postsynaptic receptor trafficking underlying a form of associative learning. Science 308:83–88.

Ryman D, Lamb BT. 2006. Genetic and environmental modifiers of Alzheimer's disease phenotypes in the mouse. Curr Alzheimer Res 3:465–473.

Segal M. 2005. Dendritic spines and long-term plasticity. Nat Rev Neurosci 6:277–284.

Sekino Y, Kojima N, Shirao T. 2007. Role of actin cytoskeleton in dendritic spine morphogenesis. Neurochem Int 51:92–104.

Selkoe DJ. 2002. Alzheimer's disease is a synaptic failure. Science 298: 789–791.

Selkoe DJ, Schenk D. 2003. Alzheimer's disease: molecular understanding predicts amyloid-based therapeutics. Annu Rev Pharmacol Toxicol 43: 545–584.

Shankar GM, Bloodgood BL, Townsend M, Walsh DM, Selkoe DJ, Sabatini

BL. 2007. Natural oligomers of the Alzheimer amyloid-beta protein induce reversible synapse loss by modulating an NMDA-type glutamate receptor-dependent signaling pathway. J Neurosci 27:2866–2875.

Shen J, Kelleher RJ 3rd. 2007. The presenilin hypothesis of Alzheimer's disease: evidence for a loss-of-function pathogenic mechanism. Proc Natl Acad Sci U S A 104:403–409.

Shi SH, Hayashi Y, Petralia RS, Zaman SH, Wenthold RJ, Svoboda K, Malinow R. 1999. Rapid spine delivery and redistribution of AMPA receptors after synaptic NMDA receptor activation. Science 284:1811–1816.

Shim KS, Lubec G. 2002. Drebrin, a dendritic spine protein, is manifold decreased in brains of patients with Alzheimer's disease and Down syndrome. Neurosci Lett 324:209–212.

Shiraishi Y, Mizutani A, Mikoshiba K, Furuichi T. 2003. Coincidence in dendritic clustering and synaptic targeting of homer proteins and NMDA receptor complex proteins NR2B and PSD95 during development of cultured hippocampal neurons. Mol Cell Neurosci 22:188–201.

Shirao T, Sekino Y. 2001. Clustering and anchoring mechanisms of molecular constituents of postsynaptic scaffolds in dendritic spines. Neurosci Res 40:1–7.

Shirao T, Kojima N, Obata K. 1992 Cloning of drebrin A and induction of neurite-like processes in drebrin-transfected cells. Neuroreport 3:109–112

Takahashi H, Sekino Y, Tanaka S, Mizui T, Kishi S, Shirao T. 2003. Drebrin-dependent actin clustering in dendritic filopodia governs synaptic targeting of postsynaptic density-95 and dendritic spine morphogenesis. J Neurosci 23:6586–6595.

Takahashi H, Mizui T, Shirao T. 2005. Down-regulation of drebrin A expression suppresses synaptic targeting of NMDA receptors in developing hippocampal neurones. J Neurochem 97 Suppl 1:110–5.

Trachtenberg JT, Chen BE, Knott GW, Feng G, Sanes JR, Welker E, Svoboda K. 2002. Long-term in vivo imaging of experience-dependent synaptic plasticity in adult cortex. Nature 420:788–794.

Trinchese F, Liu S, Battaglia F, Walter S, Mathews PM, Arancio O. 2004. Progressive age-related development of Alzheimer-like pathology in APP/PS1 mice. Ann Neurol 55:801–814.

Zuo Y, Lin A, Chang P, Gan WB. 2005. Development of long-term dendritic spine stability in diverse regions of cerebral cortex. Neuron 46:181–189.

Available online at www.sciencedirect.com
ScienceDirect
Neuroscience Research 58 (2007) 1–5
Neuroscience Research
www.elsevier.com/locate/neures

Update article

Synaptic dysfunction and disruption of postsynaptic drebrin–actin complex: A study of neurological disorders accompanied by cognitive deficits

Nobuhiko Kojima, Tomoaki Shirao *

Department of Neurobiology and Behavior, Gunma University Graduate School of Medicine, Maebashi 371-8511, Japan

Received 12 December 2006; accepted 1 February 2007
Available online 11 February 2007

Abstract

Many neurological disorders accompanied by cognitive deficits, including Alzheimer's disease (AD) and Down syndrome, exhibit abnormal dendritic spine morphology. Actin-based cytoskeletal network dynamics is critical for the regulation of spine morphology and function. Recent experimental data from an AD animal model revealed that defects in intracellular signaling cascades related to the accumulation of amyloid β (Aβ) peptide cause disruption of the postsynaptic actin-regulatory machinery, including cofilin and drebrin. The level of postsynaptic drebrin, a major F-actin-binding protein in dendritic spines, correlates well with the severity of cognitive impairment. We propose that an imbalanced regulation of the actin-regulatory machinery (loss of drebrin and increase of dephosphorylated cofilin) results in synaptic dysfunction, which underlies the cognitive impairment accompanying neurological disorders and normal aging.

Keywords: Alzheimer's disease; Amyloid β peptide; Cognitive deficits; Dendritic spines; Actin cytoskeletal network; Drebrin; Glutamate receptors

1. Introduction

Dendritic spines are small protrusions on the postsynaptic side of excitatory synapses. Within these spines are neurotransmitter receptors, ion channels, scaffolding proteins, actin cytoskeletal proteins, and intracellular signaling molecules. Abnormal spine morphology is observed in many neurological disorders accompanied by cognitive deficits, such as Alzheimer's disease (AD), Down syndrome, and fragile X syndrome (Fiala et al., 2002), suggesting that spine morphology is closely associated with spine function and that abnormal spine morphology induces the neurological symptoms of such disorders.

Actin filaments, which consist of actin molecules and actin-binding proteins, form cytoskeletal networks within dendritic spines and play critical roles in spine morphogenesis, maintenance, and plasticity (Matus, 2000; Carlisle and Kennedy, 2005; Tada and Sheng, 2006). In addition to the presence of extracellular senile plaques and intracellular neurofibrillary tangles, another prominent feature of AD is the formation of pathognomonic rod-shaped inclusions in neuronal processes called Hirano bodies, which are inclusions that contain actin and several actin-binding proteins (Galloway et al., 1987). Immunohistochemical study shows that cofilin, which binds and severs F-actin, is a major component of Hirano bodies (Maciver and Harington, 1995). Hirano bodies also show strong diffuse immunostaining for fractin, a caspase-cleaved actin fragment (Rossiter et al., 2000). These findings suggest that a defect in the actin-regulatory machinery is an underlying factor in dendritic and synaptic dysfunctions in AD. In contrast to an increased level of cofilin (Zhao et al., 2006), the level of drebrin, another actin-binding protein, is substantially decreased in AD (Harigaya et al., 1996; Hatanpaa et al., 1999).

2. Drebrin as a key regulator of spine morphology and function

Drebrin is an F-actin-binding protein that is highly expressed in the brain (Hayashi et al., 1996). Drebrin regulates the dynamics of actin cytoskeletal networks by inhibiting actin-myosin interactions (Hayashi et al., 1996; Cheng et al., 2000) and by competing for F-actin binding with other actin-binding proteins, such as tropomyosin and α-actinin (Ishikawa et al., 1994).

* Corresponding author.
E-mail address: tshirao@med.gunma-u.ac.jp (T. Shirao).

0168-0102/$ – see front matter
doi:10.1016/j.neures.2007.02.003

Drebrin A is a neuron-specific isoform (Kojima et al., 1988) and is abundantly found within spines that are located postsynaptic to only excitatory synapses (Aoki et al., 2005). The overexpression of drebrin A induces the elongation of spines in mature neurons (Hayashi and Shirao, 1999) and the change of dendritic filopodia into aberrantly enlarged megapodia in immature neurons (Mizui et al., 2005). Conversely, the suppression of drebrin A expression reduces spine density and results in the formation of thin immature spines (Takahashi et al., 2006). These findings indicate that the drebrin–actin complex plays a pivotal role in the regulation of spine morphology.

In addition to its role in regulating spine morphology, drebrin A and its accumulation within spines are required to induce the accumulation of a glutamate receptor scaffolding protein, PSD-95, at postsynaptic sites in vitro (Takahashi et al., 2003). Furthermore, the following associations between drebrin and *N*-methyl-D-aspartate (NMDA) receptors have recently been demonstrated: the activation of NMDA receptors induces the translocation of drebrin from spines to their parent dendrite (Sekino et al., 2006). Drebrin A is necessary for the homeostatic synaptic accumulation of NMDA receptors (Takahashi et al., 2006).

The proportion of drebrin-immunopositive spines in vivo is fairly constant; about 75% of spines in the adult rat cerebral cortex are immunoreactive for drebrin A (Aoki et al., 2005). However, the proportion of drebrin-immunopositive spines is regulated in an activity-dependent manner: blockade of NMDA receptor activity for two hours increases the proportion of drebrin-immunopositive spines (Fujisawa et al., 2006). Thus, drebrin may act as a key regulator of not only spine morphology but also spine function, such as synaptic plasticity.

3. Pathological changes in drebrin level in neurological disorders accompanied by cognitive deficits

We were the first to observe that drebrin disappears from the hippocampus of AD patients (Harigaya et al., 1996). Further study demonstrated that the disappearance of drebrin is not restricted to the hippocampus but also occurs throughout the cerebral cortex (Hatanpaa et al., 1999). In contrast to the marked postsynaptic changes in drebrin level occurring in AD, presynaptic changes in the content and distribution of synaptophysin are not so evident. These asymmetric changes in presynaptic and postsynaptic proteins indicate that synaptic dysfunction may result in cognitive impairment in certain neurological disorders, even if neuronal cell death and synapse loss have not yet occurred.

Similar to in AD, a decrease in drebrin level is also observed in Down syndrome (Shim and Lubec, 2002). Recently, drebrin gene expression has been reported to be activated by a basic helix-loop-helix (bHLH)–Per-Arnt-Sim (PAS) transcriptional factor, NXF, that competes with another bHLH–PAS transcriptional factor, Sim2, for the regulatory DNA elements on the drebrin gene (Ooe et al., 2004). Because Sim2 is thought to be involved in the pathogenesis of some of the morphological features and brain abnormalities observed in Down syndrome (Dahmane et al., 1995), drebrin may be directly associated with the pathogenesis of Down syndrome.

In neurological disorders accompanied by mild cognitive impairment (MCI), drebrin level is decreased in the superior temporal cortex although it remains unchanged in most cortical regions. A stepdown effect in drebrin content is observed in the superior temporal cortex from no cognitive impairment to MCI and to AD. Furthermore, drebrin level likely correlates with the severity of cognitive impairment, which is assessed antemortem using the Mini-Mental State Examination (Counts et al., 2006). On the other hand, drebrin level is increased in the superior frontal cortex in MCI. This might be explained as a compensatory response to the reduced synaptic function in MCI, although the molecular mechanism of this process is not yet known. Together, the difference in the drebrin level between cortical regions may account for the preservation of certain cognitive functions in MCI patients. Interestingly, a significant decrease in the drebrin level occurs during normal aging (Hatanpaa et al., 1999). Taken together, these findings indicate that drebrin is involved at the molecular level in the cognitive decline observed in neurological disorders as well as in normal aging.

4. Accumulation of amyloid β (Aβ) peptide induces changes in levels of actin-binding proteins, cofilin and drebrin, in Tg2576 transgenic mice

Because detailed analysis of the molecular mechanisms underlying synaptic dysfunction in various neurological disorders is difficult to perform using postmortem human tissue, many laboratories have generated genetically modified mice that mimic some symptoms of a particular neurological disorder. A useful mouse model of AD is the transgenic mouse Tg2576, which harbors the amyloid precursor protein (APP) transgene with a Swedish mutation (βAPP695.K595N/M596L) (Hsiao et al., 1996). The brains of aged Tg2576 mice accumulate Aβ peptide without inducing neuronal cell loss and neurofibrillary tangles. Paralleling the accumulation of Aβ peptide is a marked decline in the drebrin level with no significant change in the synaptophysin level (Calon et al., 2004). Cofilin level, however, is increased, and intense immunostaining of cofilin and fractin is observed in the dendrites of an aged Tg2576 mouse brain. A reciprocal relationship between drebrin and cofilin may be a result from the competitive binding of their N-terminal ADF-H domains with F-actin.

The actin depolymerizing activity of cofilin is downregulated by phosphorylation through the signaling cascade of the P21-activated kinase (PAK)/LIM-kinase (LIM-K) pathway (Arber et al., 1998; Yang et al., 1998). Because PAK and LIM-K activities are reduced in the brains of aged Tg2576 mice and AD patients (Zhao et al., 2006), the actin depolymerizing activity of cofilin may be upregulated in these brains. Interestingly in cultured hippocampal cells, the overexpression of active PAK prevents drebrin loss resulting from the treatment with soluble Aβ1–42 oligomers, whereas the intracerebroventricular infusion of a PAK inhibitor causes drebrin loss and pronounced memory deficits in normal mice (Zhao et al., 2006). Thus, the downregulation of PAK is sufficient to cause the defects